NOAA Technical Memorandum ERL WPL-153

NOAA X-BAND RADAR MEASUREMENTS IN 3CPO

Brooks E. Martner
A. Shelby Frisch
Robert A. Kropfli

Wave Propagation Laboratory
Boulder, Colorado
October 1988

NOAA Technical Memorandum ERL WPL-153

NOAA X-BAND RADAR MEASUREMENTS IN 3CPO

Brooks E. Martner
A. Shelby Frisch
Robert A. Kropfli

Wave Propagation Laboratory
Boulder, Colorado
October 1988

UNITED STATES
DEPARTMENT OF COMMERCE

C.William Verity
Secretary

NATIONAL OCEANIC AND
ATMOSPHERIC ADMINISTRATION

William E. Evans
Under Secretary for Oceans
and Atmosphere/Administrator

Environmental Research
Laboratories

Vernon E. Derr,
Director

NOTICE

Mention of a commercial company or product does not constitute an endorsement by NOAA Environmental Research Laboratories. Use for publicity or advertising purposes of the information from this publication concerning proprietary products or tests of such products is not authorized.

CONTENTS

ABSTRACT

The NOAA Wave Propagation Laboratory participated in the Cloud Chemistry Cloud Physics Organization (3CPO) field Project in east-central Illinois in the summer of 1988. The Laboratory planned to use its circular polarization diversity Doppler X-band radar to study venting of polluted boundary layer air by convective clouds using a new technique known as TRACIR. The technique and the experimental plan are described and a summary of the radar operations is given. Unfortunately, a severe drought prevented the necessary clouds from forming during the project. Numerous measurements were made with the radar in clear air conditions using vertical scans and the velocity azimuth display (VAD) method to obtain data on turbulence characteristics of the planetary boundary layer. The VAD measurements and analysis procedures are described as well as a test of the efficiency of the NOAA airborne chaff cutters. The complete radar tape log for the project is included.

1. Introduction

The Cloud Chemistry Cloud Physics Organization (3CPO) field project was conducted near Champaign, Illinois, in June 1988. It was a cooperative convective storms measurement program which involved scientists from several U.S. laboratories, universities and the Illinois State Water Survey. The principal objective was "to provide as complete a description as is technically possible of the dynamical, microphysical and chemical processes occurring within convective storms" (Sisterson, 1987).

The project was scheduled to take place in east-central Illinois in the summer of 1988 in order to coincide with the precipitation scavenging field study (PRECP VI) of the National Acid Precipitation Assessment Program and with planned weather modification research of the Precipitation Augmentation for Crops Experiment. In addition to the opportunity to share expensive facilities, the Illinois site was selected partly on the basis of its proximity to regional air pollution sources and the climatological likelihood of numerous thunderstorms in June. As sometimes happens, however, the gathering of atmospheric scientists and instruments did not coincide with gathering clouds in this case.

June 1988 was, in fact, the driest June on record at Champaign-Urbana (see news article in Appendix A) as the worst drought since the "dust bowl" years of the 1930's gripped the midwestern states. Champaign received only 8% of its normal 4.0 inches of June rainfall. Incredibly, throughout June and well into July there were almost no convective clouds larger than fair weather cumuli. Many days were completely cloudless.

As part of 3CPO, the NOAA Wave Propagation Laboratory (WPL) was to have conducted a study of venting of boundary layer air by convective clouds using a new radar technique. The experiment which is described in more detail in the next section uses circularly polarized radar to track chaff-tagged air parcels as they are drawn from the boundary layer by updrafts into and through vigorous convective clouds. The radar chaff fibers are released by an aircraft flying in the planetary boundary layer. The radar then monitors the chaff's distinctive circular depolarization ratio signal which can be detected inside cloud as well as in clear air.

The WPL experiment was funded by the Electric Power Research Institute (EPRI) and was conducted by NOAA/WPL as a subcontractor to Battelle Pacific Northwest Laboratories. A NOAA X-band Doppler radar was on station for measurements near Champaign from June 1st to July 5th. The absence of vigorous convective clouds during this period was devastating to the planned experiment. While the 3CPO research aircraft fared slightly better by venturing off to storms in neighboring states, the NOAA radar was tied to the driest part of Illinois.

In short, there were no clouds suitable for the boundary layer venting experiment, therefore, no useful radar data were obtained for that research. WPL did, however, by collect radar measurements in clear air conditions on several days and nights in Illinois. These data may be useful to ongoing NOAA radar studies of boundary layer turbulence. In addition, several test flight chaff releases were made in clear air for the purpose of improving and quantifying the chaff delivery system. Upgrades and refinements to the radar itself, especially to the color display features, were also made in during the stay in Illinois. Results of these activities are discussed briefly in this report. The data analyses presented here are merely abbreviated examples of the radar's capabilities. An in depth analysis effort has been precluded by the failure to obtain data from the boundary layer venting experiment and by the sponsor's understandable subsequent withdrawal of funding for analysis.

2. The Planned Experiment

The experiment prepared by the Wave Propagation Lab for 3CPO was an attempt to study how effectively convective clouds draw air from the polluted boundary layer and redistribute it to greater heights. This can be examined by releasing radar-reflective chaff fibers in the lower atmosphere and tracking their subsequent movements with circularly polarized radar. The depolarizing properties of chaff dipoles are very much different from those of hydrometeors. The circular depolarization ratio (CDR) signal backscattered by chaff is, for example, about 20 dB stronger than that returned by raindrops. Hence, the chaff's CDR signature can be detected and tracked within cloud as well as in the clear air. The fibers are light enough (fall speed is 0.3 m/s), that for most purposes it can be assumed that they faithfully follow the motions of the air in which they are released.

This technique, developed at WPL, is known as TRACIR (TRacking Air with Circular-polarized Radar). The theory behind the technique and some demonstrations of its feasibility are described in articles by Moninger and Kropfli (1987) and Kropfli and Martner (1988). In this report only the plan for applying the TRACIR technique to the boundary layer venting problem is described.

The 3CPO experiment called for chaff to be released from an aircraft flying in the polluted boundary layer within about 40 km of the NOAA X-band radar. The operations plan for three graduated stages of cloud development are illustrated in Figures 2.1-2.3.

In early stages of convective cloud development (Figure 2.1 - cumulus congestus) chaff would be released in a broadcast manner. This would insure that at least some chaff is in place beneath whichever clouds subsequently "take off" in vigorous

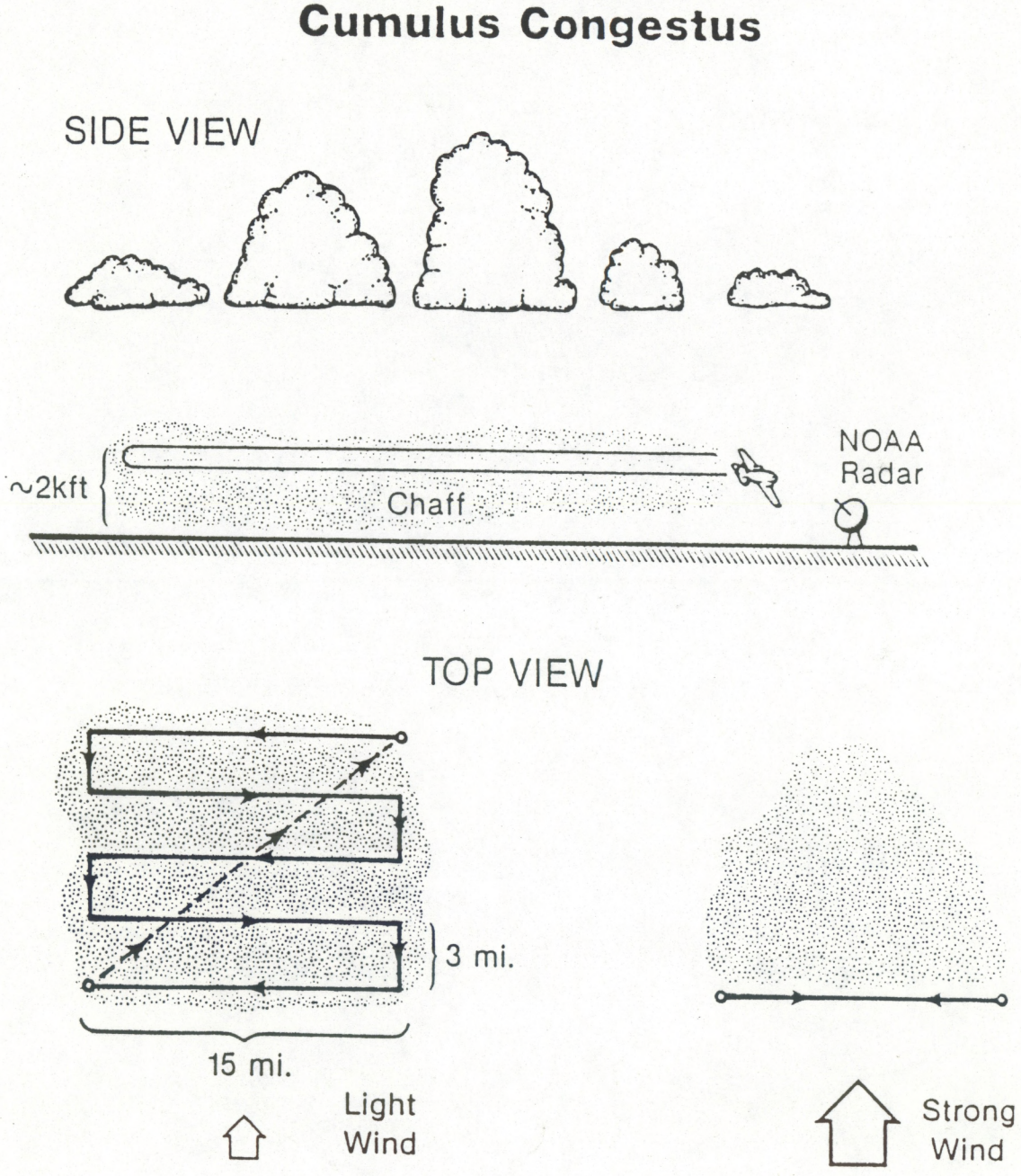

Figure 2.1. Flight plan for chaff releases in boundary layer venting experiment during early stages of cloud growth.

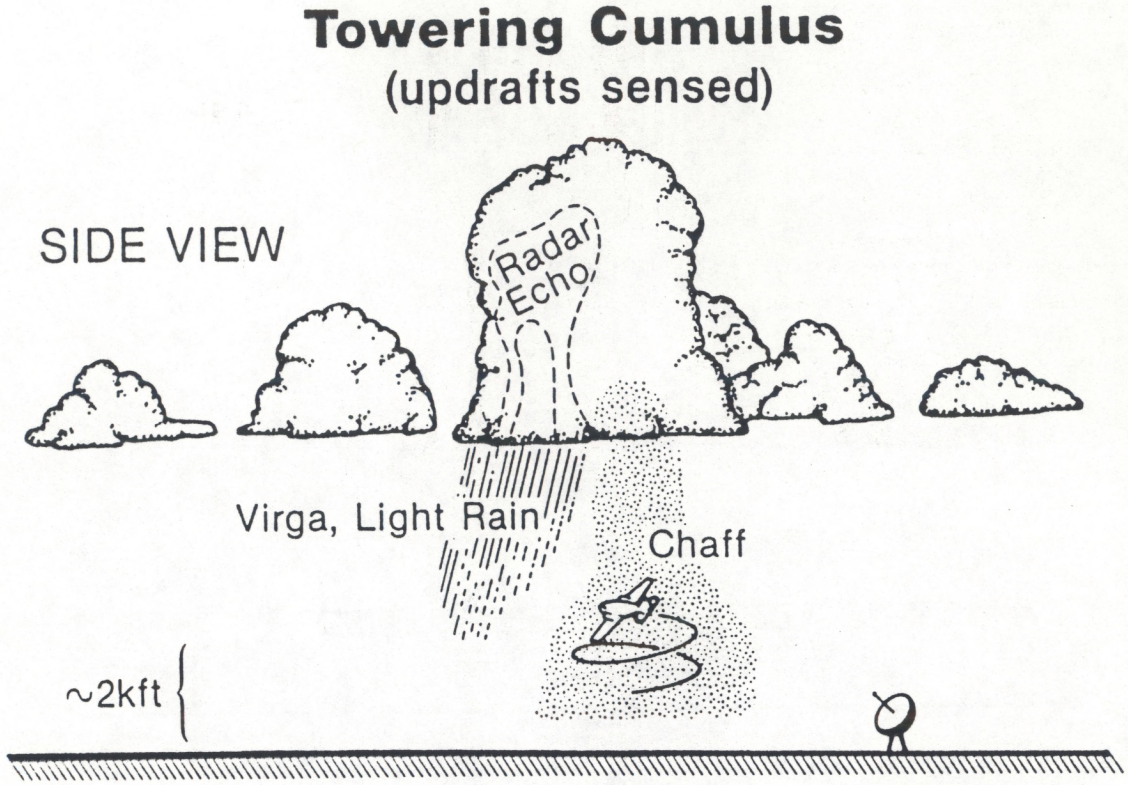

Figure 2.2. Flight plan for chaff releases in boundary layer venting experiment during towering cumulus stage.

Mature Thunderstorms

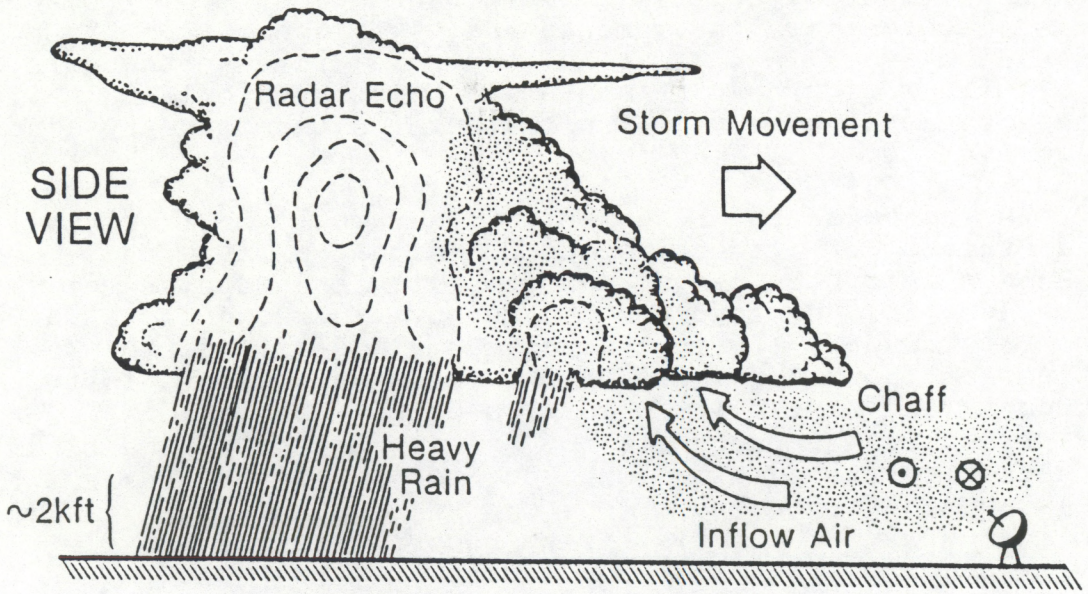

Pilot keeps shifting pattern to stay
ahead of advancing storm.

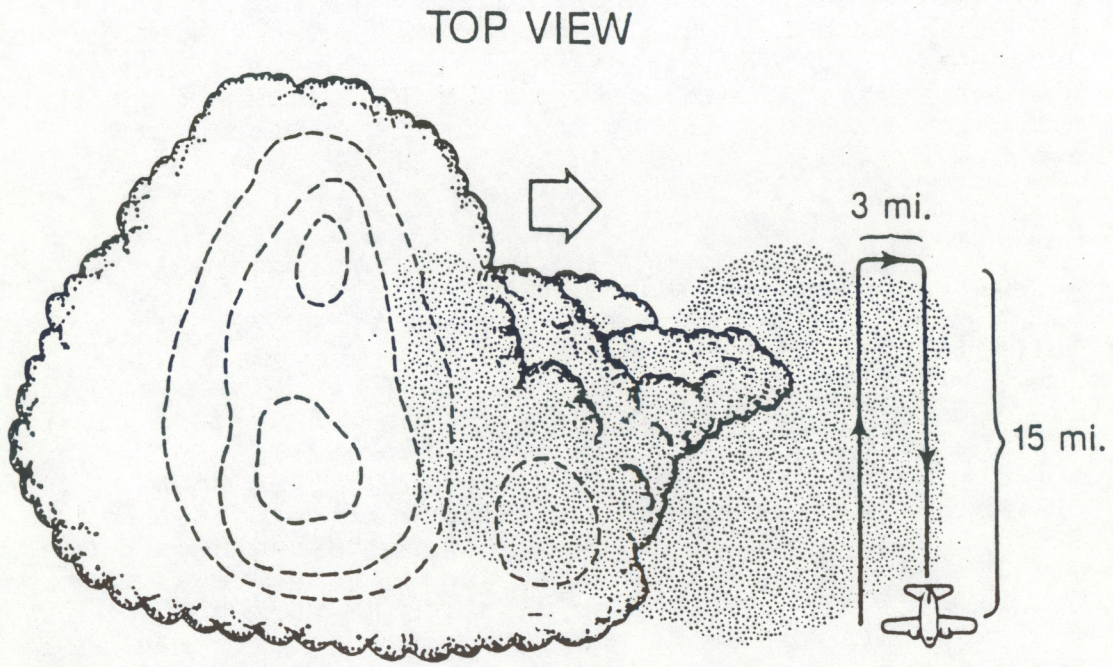

Figure 2.3. Flight plan for chaff releases in boundary layer venting experiment during intense thunderstorm or squall line stage.

vertical growth. At that point (Figure 2.2 - towering cumulus) the airplane would orbit in the boundary layer beneath a rapidly growing cloud to concentrate the chaff there. These clouds would be identified by the aircraft crew from visual appearances (flat, dark base, sharply defined "cauliflower" tops, etc.), by updrafts sensed with onboard instruments and by evidence from the NOAA radar displays. In the case of a mature, intense thunderstorm or squall line (Figure 2.3) the release aircraft would maintain transects ahead of the advancing storm in the boundary layer inflow region.

In each case the NOAA X-band radar would monitor the chaff-tagged air, recording its CDR signal along with measurements of the cloud's reflectivity and Doppler velocity patterns. If the cloud's updrafts have roots which reach deep into the boundary layer, the radar could easily detect the upward motions of the chaff-filled air parcels as they are lofted through cloud base. It could also detect subsequent redistribution of the chaff to various regions of the cloud and perhaps also its eventual exhaust back to the clear air. Flux rates and chaff concentrations can be computed under favorable conditions from the reflectivity recorded in the radar's cross-polarized channel.

In the 3CPO Operations Plan (Daum, et al., 1988) Battelle Labs' Gulfstream-I was slated to release the chaff while simultaneously measuring concentrations of numerous pollutants in the boundary layer air. The project's precipitation network at the ground collected timed rainwater samples for various chemical analyses. Thus, pollutant levels in the air prior to a thunderstorm and in the rainwater following the storm would be documented. The NOAA radar would provide the kinematic link between those two data sets with a 3-D picture of trajectories of air parcels tagged in the boundary layer with chaff.

3. Work Conducted in 3CPO

A. Logistical

Operating characteristics of the NOAA X-band radar as it was configured for 3CPO are listed in Table 3.1. In March, 1988, WPL selected a field site for the radar near the town of Ivesdale, Illinois, 22 km southwest of Willard Airport as shown in Figure 3.1. Located on flat farmland, the site had a good radar horizon with no beam blockage problems from nearby trees or structures. It was within the 3CPO precipitation network and was far enough from the CHILL radar to permit a moderate size region for coordinated dual-Doppler radar measurements of storms. However, it was close enough to the operations center and chaff airplane base at the airport to facilitate logistics.

****

TABLE 3.1

CHARACTERISTICS OF THE NOAA-C RADAR

****

Frequency: 9.3 GHz (X-band)
Wavelength: 3.2 cm
Peak transmitted power: 33 kw ** (up to 50 kw possible)
PRP: 400 and 1600 microseconds ** (double pulse system is used for distinguishing 2nd trip targets)
MDS at 25km: -10 dBZ (linear receiver) **
Polarization: circular (main and cross-polarized measured)
Beam width: 0.8 degrees
Antenna: 3 meter parabolic reflector with circular cross section
Scan types: PPI, sector, RHI, zenith, coplane and fixed beam
Pulse width: adjustable, 1 microsecond (150 m) is typical

Range gate spacing, azimuth, elevation steps & limits: extremely flexible; operator can alter with a few keystrokes
Scan rates: very flexible, fastest rate depends on size of sector
Parameters measured: reflectivity (main & cross), radial velocity, variance of Doppler spectra, circular depolarization ratio (CDR), correlation, and Doppler spectra in a separate mode
Doppler processing: pulse pair processor or time series techniques

Data system: Data General S-120 computer controls antenna operation, recording and displays through NOAA's Radar Control Program (Moninger, 1983). Hundreds of pre-programmed optimized scans can be called from the disk for immediate use.
Data recording: Two Kennedy 1600 bpi tape drives which ping-pong from one to the other at the end of tapes. VCR documents visual weather features in direction of radar beam.
Real time displays: color monitor of reflectivity, radial velocity, CDR and correlation patterns; A-scope displays of received power in linear and both log channels; TV monitor of weather along direction of beam from video camera on antenna; coordinated universal time digital clock; digital displays of beam azimuth and elevation angles; field tapes can be played back through color monitor.

** = values used in 1988 field season; these can be altered under some circumstances to better suit the needs of individual experiments.

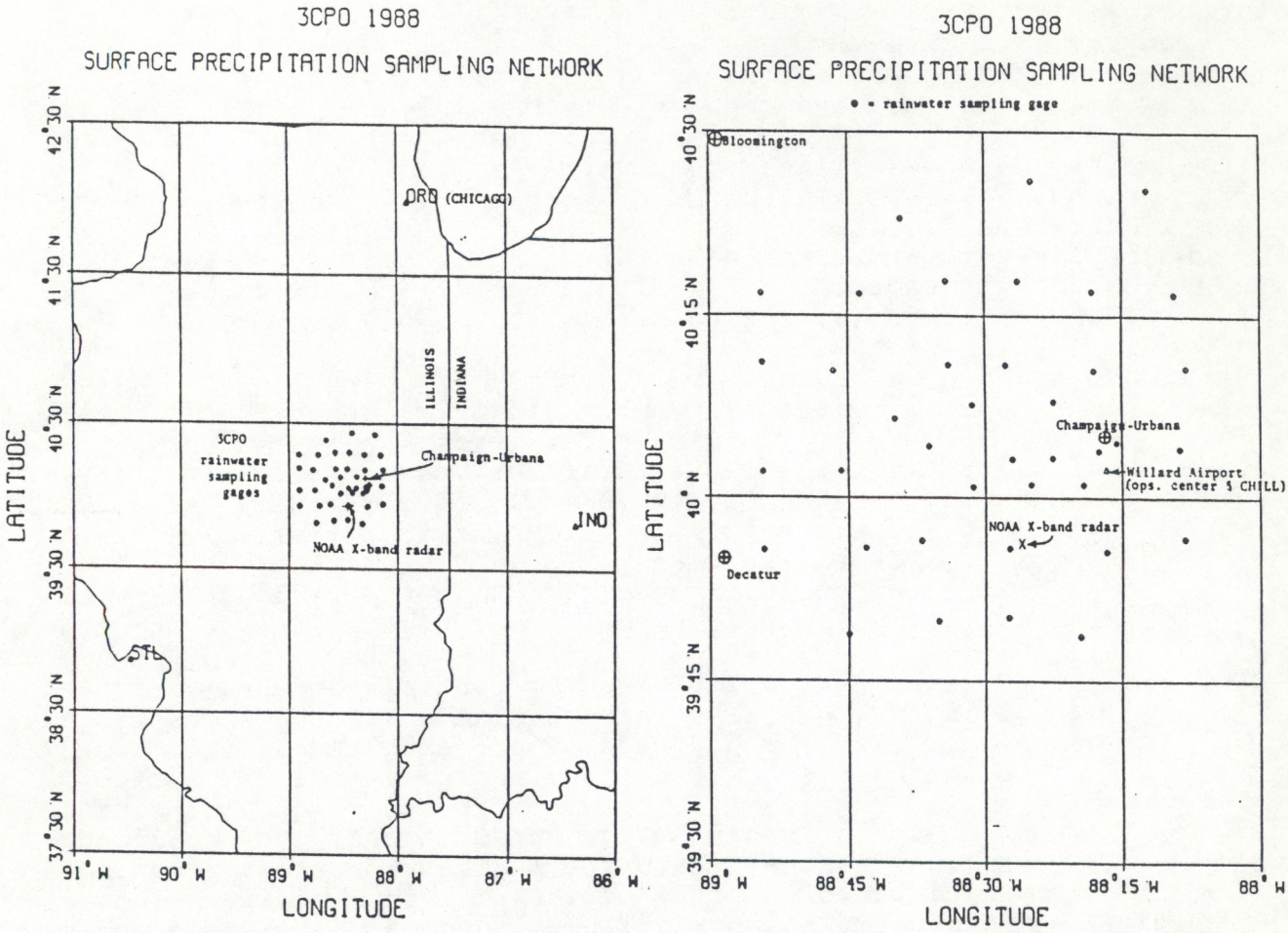

Figure 3.1. Facilities location map for 3CPO project. (Courtesy of Joyce Tichler, Brookhaven National Lab).

The radar arrived on site in late May and was prepared for full operations by June 1st. It remained on site through July 5th. Sun observations were conducted to insure the accuracy of the radar's pointing angles. A full receiver calibration was performed on June 10th; it showed virtually no change from the previous calibration just prior to leaving Colorado. Synchronization tests of programmed scans for dual-Doppler scanning with CHILL were also conducted in the field, but the scans were not used because of the lack of storms and other priorities for both radars.

Less than a month before the start of the field project, Battelle's Gulfstream research aircraft suffered an accident on the ground which prevented it from taking part in the project. Since the Gulfstream was to have released the chaff for the WPL experiment, it was necessary to find a substitute chaff release airplane on very short notice. WPL chose a Cessna-210 Centurion operated by the NOAA Office of Aircraft Operations in Miami. OAO installed two chaff cutters in the baggage area of the airplane and it arrived in Champaign on the evening of June 2nd. Numerous test flights were made to exercise the chaff cutters and correct problems in this untested airplane/chaff system configuration. The rear cutter in particular frequently jammed until the problem was eventually solved by enlarging the cutter's air inlet aperture inside the airplane.

The Cessna-210 was not equipped for atmospheric research, therefore, it was necessary to rent a small data system for it. The data system was provided and installed by Science Engineering Associates. Each second it recorded the aircraft's location, altitude, and whether each chaff cutter was turned on or off. The first flight with the data system onboard was on June 7th. A sample flight track produced from the chaff airplane data system is shown in Appendix A.

B. Data Collection

A list of all magnetic data tapes from the NOAA X-band radar operations during 3CPO is given in Appendix A. The tapes include radar measurements during several chaff airplane test flights in clear air, measurements made in clear conditions for boundary layer turbulence studies, trial run chaff releases beneath very weak clouds, and special measurements such as calibrations and ground clutter patterns. By the end of July all of the field raw data tapes had been processed to produce common Doppler radar data exchange format ("universal format") tapes (Barnes, 1980) which are archived along with the field tapes at NOAA/WPL.

Although towering cumulus clouds suitable for the boundary layer venting experiment never did appear during the drought, some practice runs were conducted with obviously inferior clouds. Chaff was released in the broadcast manner or beneath individual fair weather cumuli on June 15th, 24th and 29th. These clouds did not produce precipitation, but very weak radar echoes were sometimes detected. By monitoring the CDR patterns on the

real-time color display it was evident that the the chaff showed no sign of rising into the clouds. Instead, it remained within the boundary layer where it diffused and very slowly settled downward. Clearly, these clouds were insignificant factors in removing air and pollutants from the low atmosphere. This is to be expected of such placid clouds which have very weak, shallow updrafts.

Chaff was also released ahead of and within a widespread stratus rainstorm on June 8th. This was the only day Champaign-Urbana received measurable rainfall during the project. The storm began two days earlier in Colorado and became a mesoscale convective complex over Nebraska. It had greatly deteriorated, however, into a uniform rain region by the time it reached the 3CPO network. Except for a prominent melting layer bright band, the storm's reflectivity pattern was quite uniform, indicating the absence of significant convection. Once again the CDR measurements showed that the chaff did not rise into the storm which by this time must have been dominated by gentle downdrafts. The chaff airplane pilot reported an extremely smooth flight.

WPL did utilize many of the hot clear days and nights to collect Doppler measurements for ongoing studies of boundary layer turbulence. Measurements were made in the velocity azimuth display (VAD) and vertical scanning modes using the plentiful insects in the boundary layer for scattering targets. The technique is described in the next section where an example of the Illinois data is presented. The turbulence measurements were made on June 6th, 7th, 11th, 12th, 13th, 14th, 18th, 23rd, 24th and July 1st.

On June 25th and July 1st radar measurements of the clear air were recorded in a special time series mode. These data will be useful in a continuing study of radar signal processing in which a comparison of the conventional pulse-pair method is made with a more sophisticated time series technique for computing moments of the Doppler velocity spectrum.

Special test flights were made on three days (June 7th, 9th and 25th) to obtain radar measurements of chaff concentrations in clear air. The purpose of the tests was to examine how effectively the airborne chaff releases produce unaggregated single fibers of chaff. This information will be useful for assessing future improvements to the chaff release system which will allow the TRACIR technique to be used in more intense precipitation than is now feasible. The data from one of these cases is analyzed in Section 5.

4. Clear Air Boundary Layer Studies

a. Background

Special scanning procedures were used on several fair weather days and nights during 3CPO to obtain measurements of the airflow and turbulence structure of the planetary boundary layer. These data may be incorporated in ongoing studies of boundary layer meteorology by NOAA/WPL. The measurements have practical applications to air pollution diffusion research, earth-atmosphere energy exchanges, climate modeling and other fields. In this section the techniques are summarized and a preliminary analysis of one of the Illinois cases is presented.

Boundary layer profiles of turbulent wind stress, variances, and mean winds can be derived from single Doppler radar data by using suitable scanning analysis techniques. These scanning and analysis methods have been discussed in detail by Lhermitte (1968), Browning and Wexler (1969), Wilson (1970), and Kropfli (1986). The scatterers that are used as air motion tracers occur naturally. They are present in the air during strong upward heat flux in the summer in many continental locations and are believed to be insects, seeds and other millimeter sized particles (Kropfli, 1986). The velocity azimuth display (VAD) method described below employs full 360-degree azimuth sweeps at constant elevation angles to measure mean and turbulent velocities. By the choice of appropriate elevation angles, the method can be used to compute the vertical flux of turbulent kinetic energy at the different measurement heights.

b. Method

Browning and Wexler (1968) developed the VAD method to measure wind speed and direction by scanning the radar at a constant elevation angle above the ground. By fitting a Fourier series to the measured radial velocities as a function of azimuth at a fixed radar range and assuming a mean linear gradient of the local wind, they could relate the first harmonic coefficients to the mean wind speed and direction. The same conical scan was used by Wilson (1970) to measure several second-moment quantities. He measured the variance of the Doppler velocity around a circle, and computed $\overline{u'v'}$, $\overline{u'w'}$, $\overline{v'w'}$, $\overline{u'^2 + v'^2}$, and $\overline{w'^2}$, where u, v, and w are defined in the conventional sense; the primes indicate deviations from the mean; and the overbars denote a spatial average. To make this calculation, he had to assume that the statistical quantities were horizontally homogeneous. To further ensure this assumption of horizontal homogeneity, and to expand the range of horizontal scales included in the estimates, Kropfli (1986) extended Wilson's analysis by averaging several scans taken during periods of 20 minutes or longer. In this study Kropfli's averaging technique is used to determine both the average wind speed and direction, as well as several second-moment turbulence terms. It is shown how the technique can be extended to measure the vertical flux of turbulent kinetic energy.

i. Relationship between the radial velocity and the wind

Figure 4.1 shows the scanning geometry used for this radar analysis, and Fig. 4.2 shows a sample of the measured radial velocity. The relationship between the radial

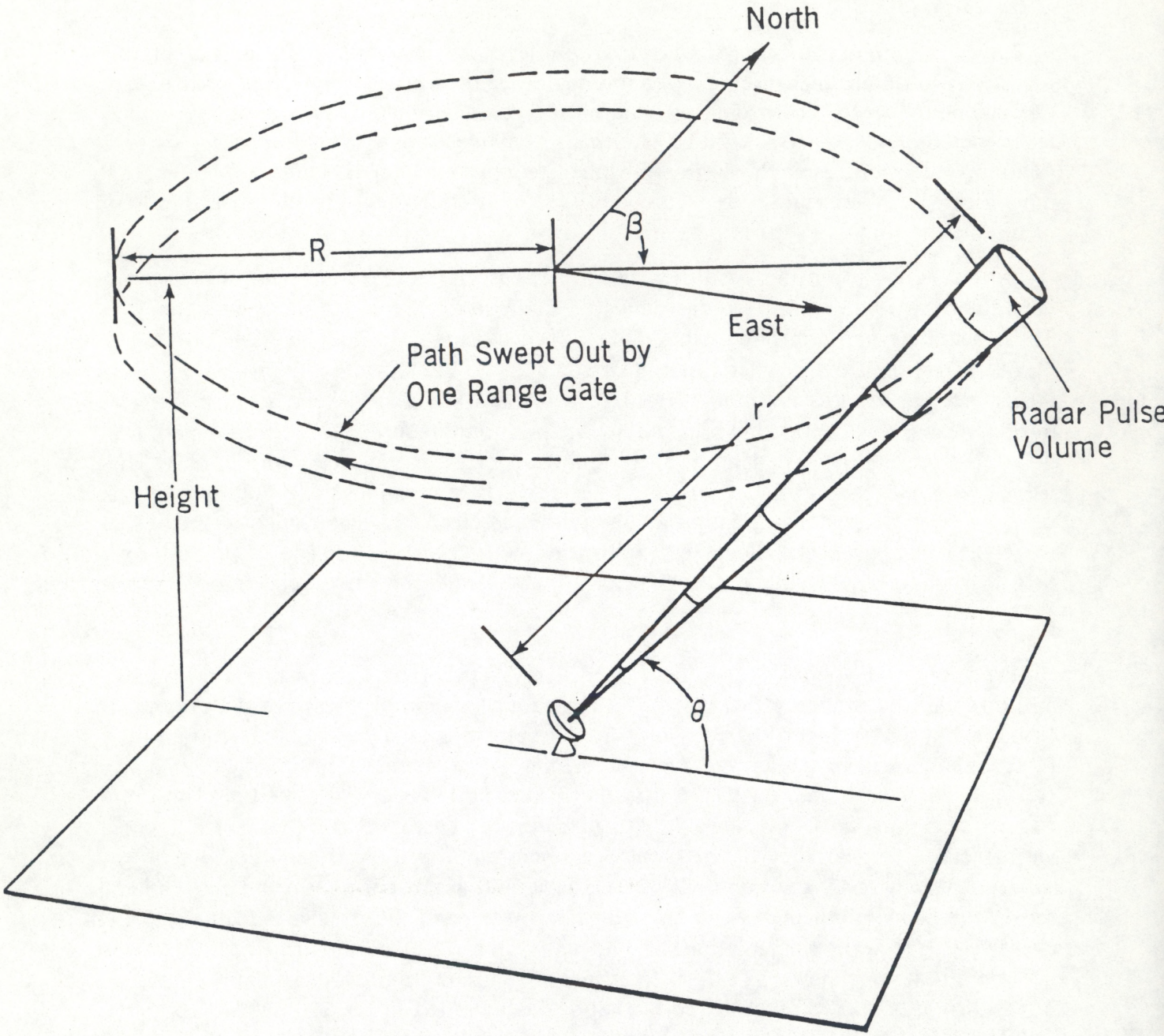

Figure 4.1. Scanning geometry for velocity azimuth display method.

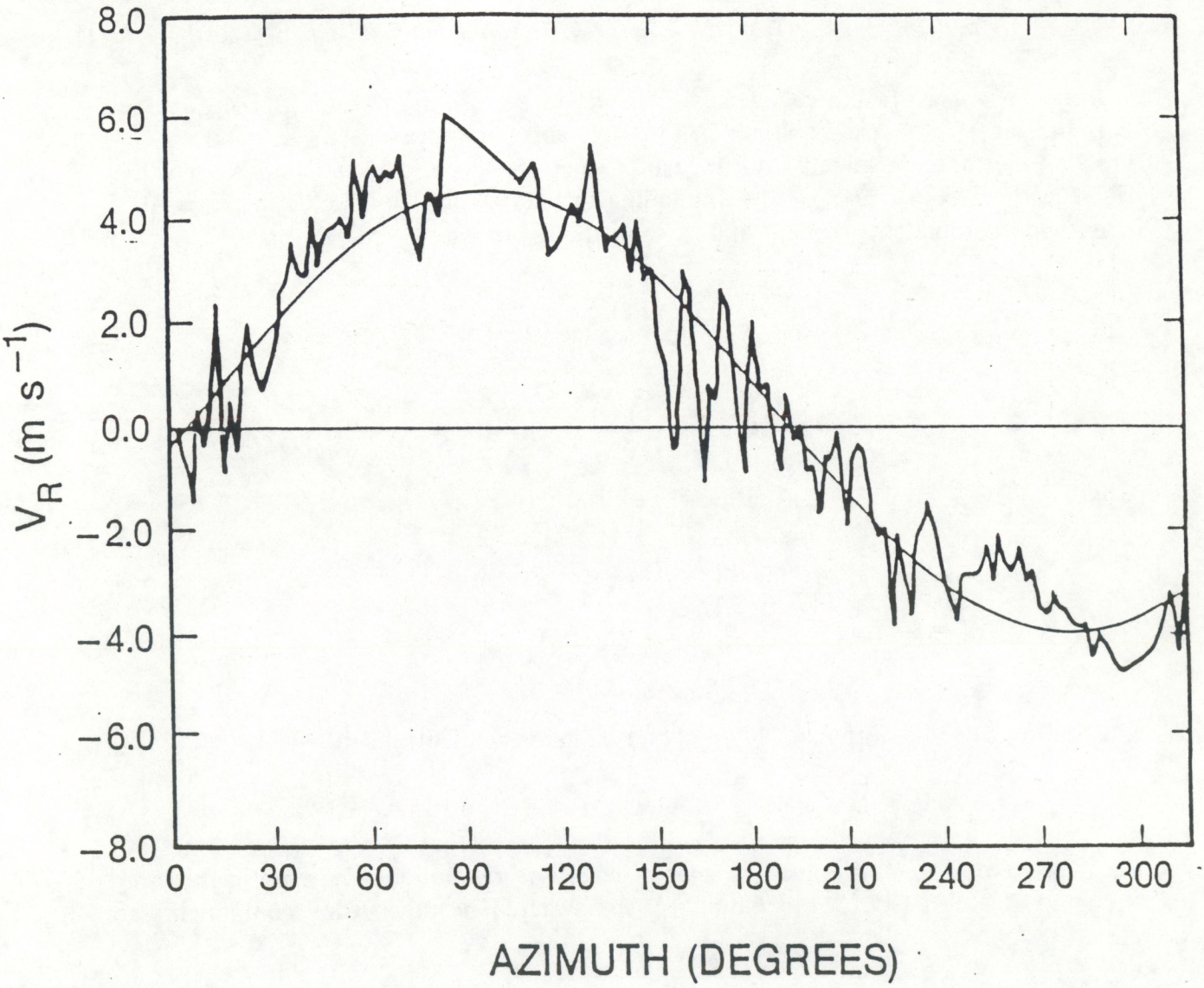

Figure 4.2. Typical sample of radial velocities measured as a function of azimuth for one range gate (one height) at a constant elevation sweep in the VAD method.

velocity and the mean wind at fixed range R, is given by the following (after Browning and Wexler (1969)):

$$V_R(\beta, \theta, t) = u(\beta, \theta, t) \sin\beta\cos\theta + v(\beta, \theta, t) \cos\beta\cos\theta + w(\beta, \theta, t) \sin\theta , \qquad (1)$$

where u, v, and w are the velocity components in the east-north zenith coordinate system, and where β, θ are as shown in Fig. 4.1, and t is time. The mean wind speed and direction can be determined from measurements of V_R, defined as positive for velocities receeding from the radar, by expanding the horizontal wind fields in terms of mean wind components u_o, v_o, and w_o and the mean wind gradients as

$$u = u_o + x\left(\frac{\partial u}{\partial x}\right) + y\left(\frac{\partial u}{\partial y}\right) \qquad (2a)$$

$$v = v_o + x\left(\frac{\partial v}{\partial x}\right) + y\left(\frac{\partial v}{\partial y}\right) \qquad (2b)$$

where

$$w = w_o \qquad (2c)$$

$$x = R \sin\beta\cos\theta$$

$$y = R \cos\beta\cos\theta$$

Substituting Eqs. (2) into Eq. (1) yields an equation with the form

$$\overline{V_R(\beta, \theta, t)} = A_{0t} + A_{1t} \sin\beta + A_{2t} \cos\beta + A_{3t} \sin 2\beta + A_{4t} \cos 2\beta . \qquad (3)$$

The overbar represents an average over at least one revolution. The coefficients are evaluated at time t from the beginning of the sweep. The mean wind components are related to

$$A_{0t} = \frac{R}{2} \cos\theta \left(\left\langle \frac{\partial u}{\partial x} \right\rangle + \left\langle \frac{\partial v}{\partial y} \right\rangle \right) + w_o \sin\theta \qquad (4a)$$

$$A_{1t} = u_o \cos\theta \qquad (4b)$$

$$A_{2t} = v_o \cos\theta \qquad (4c)$$

$$A_{3t} = \frac{R}{2} \cos\theta \left(\left\langle \frac{\partial u}{\partial y} \right\rangle + \left\langle \frac{\partial v}{\partial x} \right\rangle \right) \qquad (4d)$$

$$A_{4t} = \frac{R}{2} \cos\theta \left(\left\langle \frac{\partial u}{\partial x} \right\rangle + \left\langle \frac{\partial v}{\partial y} \right\rangle \right) \qquad (4e)$$

ii. The second moments

The second moment of the radial velocity can be related to the second moments in the wind field by using (1) and assuming horizontal homogeneity. This gives the following relationship for the variance relationship:

$$varV_R \equiv \overline{(V_R - \overline{V_R})^2} = \overline{u'^2}\cos^2\theta\sin^2\beta + \overline{v'^2}\cos^2\theta\cos^2\beta$$

$$+\overline{w'^2}\sin^2\theta + \overline{u'v'}\cos^2\theta\sin 2\beta + \overline{u'w'}\sin 2\theta\sin\beta + \overline{v'w'}\sin 2\theta\cos\beta\,. \qquad (5)$$

Integrating the variance over four quadrants of the scanned circle, as first shown by Wilson (1970), gives

$$I_1 = \int_0^{\frac{\pi}{2}} \mathrm{var}V_R d\beta; \qquad I_2 = \int_{\frac{\pi}{2}}^{\pi} \mathrm{var}V_R d\beta$$

$$I_3 = \int_{\pi}^{\frac{3\pi}{2}} \mathrm{var}V_R d\beta; \qquad I_4 = \int_{\frac{3\pi}{2}}^{2\pi} \mathrm{var}V_R d\beta\,. \qquad (6)$$

We can solve for the momentum fluxes in (5) in terms of the integrals in (6) as

$$\overline{u'w'} = [(I_1 + I_2) - (I_3 + I_4)](4\sin 2\theta)^{-1}\,, \qquad (7a)$$

$$\overline{v'w'} = [(I_1 + I_4) - (I_3 + I_2)](4\sin 2\theta)^{-1}\,, \qquad (7b)$$

and for the variances as

$$\overline{u'^2 + v'^2} + 2\tan^2\theta\,\overline{w'^2} = (\pi\cos^2\theta)^{-1}(I_1 + I_2 + I_3 + I_4)\,. \qquad (7c)$$

At low elevation angles,

$$\overline{u'^2 + v'^2} \cong (\pi\cos^2\theta)^{-1}(I_1 + I_2 + I_3 + I_4)\,; \qquad (8)$$

at high elevation angles,

$$\overline{w'^2} = (2\pi\sin^2\theta)^{-1}(I_1 + I_2 + I_3 + I_4)\,; \qquad (9)$$

and at $\theta = 35.3°$.

$$\overline{u'^2 + v'^2 + w'^2} = 0.48(I_1 + I_2 + I_3 + I_4) \ . \tag{10}$$

iii. The third moments

As shown below, the third moment of V_R can be used to measure the vertical flux of turbulent kinetic energy as well as other higher order moments. Taking the third moment of V_R at a point, we have

$$\begin{aligned}\overline{[V_R(\theta,\beta) - \overline{V_R}(\theta,\beta)]^3} &= \overline{u'^3}\cos^3\theta\sin^3\beta + \overline{v'^3}\cos^3\theta\cos^3\beta \\ &+ 3\overline{u'^2v'}\cos^3\theta\sin^2\beta\cos\beta + 3\overline{v'^2v'}\cos^3\theta\sin\beta\cos^2\beta \\ &+ 3\overline{u'^2w'}\sin\theta\cos^2\theta\sin^2\beta + 3\overline{v'^2w'}\sin\theta\cos^2\theta\cos^2\beta \\ &+ 3\overline{u'w'^2}\sin^2\theta\cos\theta\sin\beta + 3\overline{v'w'^2}\sin^2\theta\cos\theta\cos\beta \\ &+ 6\overline{u'v'w'}\sin\theta\cos^2\theta\sin\beta\cos\beta + \overline{w'^3}\sin^3\theta \ . \end{aligned} \tag{11}$$

If we assume that the turbulence is horizontally homogeneous, and then integrate with respect to β from $\beta = 0$ to 2π, we obtain

$$\int_0^{2\pi} \overline{(V_R - \overline{V_R})^3}d\beta = 3\pi(\overline{u'^2w'} + \overline{v'^2w'})\sin\theta\cos^2\theta + 2\pi\overline{w'^3}\sin^3\theta \ . \tag{12}$$

By scanning the antenna at an elevation angle of 50.8°, the vertical flux of turbulent kinetic energy can be computed directly as

$$\overline{w'(u'^2 + v'^2 + w'^2)} \equiv \overline{w'(q^2)} = (0.93\pi)^{-1} \int_0^{2\pi} (V_R - \overline{V_R})^3 d\beta \ , \tag{13}$$

where q^2 is turbulent kinetic energy.

iv. Turbulent kinetic energy

One quantity of interest to boundary layer meteorologists is the behavior of the turbulent kinetic energy q^2. The equation for the generation of q^2 is given by (Businger, 1982)

$$\frac{1}{2}\frac{\partial \overline{q^2}}{\partial t} = -\overline{u'w'}\frac{\partial \bar{u}}{\partial z} - \overline{v'w'}\frac{\partial \bar{v}}{\partial z} + \frac{g}{\theta}\overline{\theta' w'} - \frac{\partial}{\partial z}\overline{w'(q'^2 - p')} - \epsilon \,, \qquad (14)$$

where the left hand side is the local rate of change of total turbulent kinetic energy; the first two terms on the right-hand side are the shear production terms; the third term is the buoyancy production term; the fourth term is the divergence of the turbulent transport of kinetic energy and pressure fluctuations; the fifth term is the dissipation rate of turbulent kinetic energy, θ is the potential temperature, and θ' the potential temperature fluctuation.

An alternating sequence of scans at 35° and 51° can be used to compute all but the buoyancy and the pressure terms in (14). Turbulent kinetic energy and therefore its temporal rate of change, can be computed from the 35° elevation scans as indicated by (10). Equations (7a) and (7b) can be used to compute $\overline{u'w'}$ and $\overline{v'w'}$ and (4a) and (4b) to compute u_o and v_o as a function of height from which the shear production terms are computed from both elevation angles. Equation (13) can be used to compute the vertical flux of turbulent kinetic energy as a function of height, so the flux divergence term can be evaluated from the 51° elevation scans. The turbulent dissipation rate can in principle be computed either by using the second-moment method described by Frisch and Clifford (1974) or by the first-moment method demonstrated by Frisch and Strauch (1975). A complication in the second-moment method is the possibility that there may not be enough scatterers in the radar pulse volume to estimate the spectral second moment.

c. Analysis on an Illinois Case

For the clear air boundary layer measurements in 3CPO the NOAA X-band radar was operated with a pulse length of 90 m, and a range gate spacing of 112 m out to a maximum of 4 km. The half-power beam width of the radar is 0.8 degrees. The radar scanned in a sequence of circles at elevation angles of 35.0, 50.8, and 89.0 degrees. A slow sweep rate was used; each revolution of the antenna took 1 to 2 minutes. On the hot, clear days and nights during the drought, abundant airborne insects and other natural scatterers over the Illinois farmlands backscattered relatively strong signals to the radar.

The variance of vertical velocity is an important parameter in boundary layer dispersion modeling (Misra, 1981). The profile of this parameter, computed from radar data, is shown here for measurements made from late morning to early afternoon on June 6, 1988. This was a hot, cloudless day with light surface winds. This data are normalized to a non-dimensional height Z/Z_i and vertical velocity variance $\overline{w'^2}/w_*^2$. We defined Z_i as that height above the surface layer where $\overline{w'^2}$ was a minimum. The scaling velocity sometimes called the convective velocity scale is defined as $w_* \equiv [g/T\, Q_o\, Z_i]^{1/3}$ where Q_o is the vertical heat flux at the surface. Since we had no direct estimates of Q_o, we started with Kaimal et al.'s (1976) estimates during the midday, when things were relatively constant. In this case $Q_o \sim 0.15$ °C m s^{-1}. We have

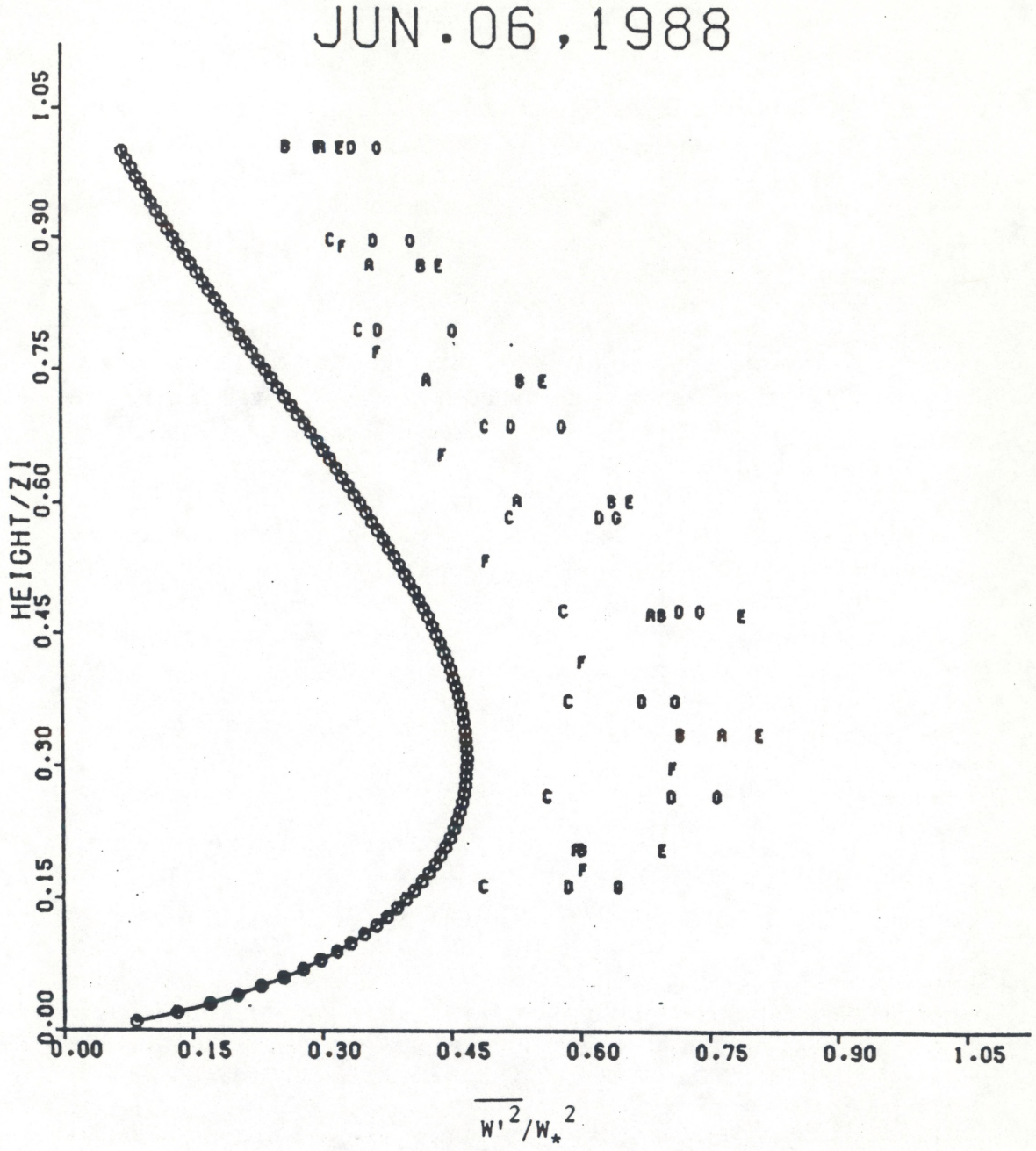

Figure 4.3. Profile of normalized variance of vertical velocity computed from VAD scans of the NOAA X-band radar on 6JUN88 near Ivesdale, IL. Each lettered point represents a 40-minute average at the indicated height. Measurements spanned the period 09:00 to 16:00 CDT. For comparison, the solid line shows aircraft measurements by Lenshow et al. (1980). See text for details.

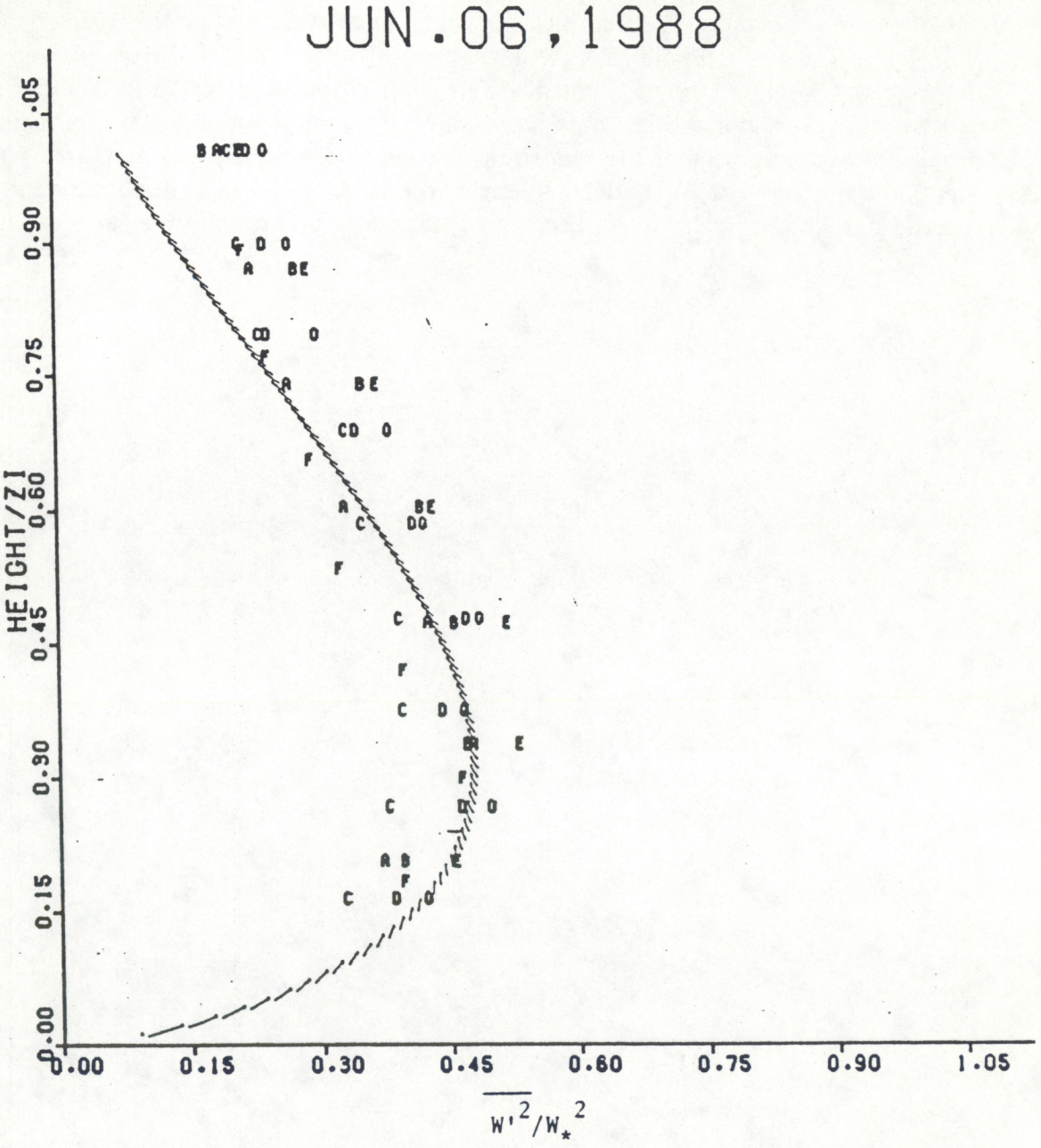

Figure 4.4. As in previous figure except a stronger surface heat flux has been used in the computations.

plotted our results using this value (Fig. 4.3). The solid curve is from Lenschow et al. (1980) which they computed empirically from aircraft data over the Western Pacific. We can adjust our estimate of Q_o for a better fit of this curve. Figure 4.4, is the result of using 0.5 °C m s^{-1} for Q_o, considerably higher than that found by Kaimal et al. (1976). However, the present data were taken on a very hot, dry day, during a record drought, so it may be that the heat flux was considerably higher than during the period that Kaimal et al. (1976) made their measurements. In spite of this uncertainty, there is good agreement in the overall shape of the curve of Lenschow et al. (1980).

5. Chaff Cutter Efficiency Test

The CDR signature of single, unaggregated chaff dipole fibers is 0 decibels. It is known from observation, however, that only a small fraction of the fibers from the WPL chaff cutters enter the airstream as single needles; the rest fall out in clumps for which the CDR value is unknown. The fraction which are unaggregated is generally sufficient for tracking air parcels in clouds with the TRACIR technique. It would be valuable, however, to increase the fraction by improving the present chaff cutter/release system. Kropfli and Martner (1988) have shown analytically that greater concentrations of unaggregated chaff fibers allows the TRACIR technique to be useful in more intensely precipitating storms. An initial step toward such improvements is to quantitatively assess the performance of the current apparatus.

A special test was conducted on June 25th to establish the effective fraction of the total number of chaff fibers that scattered as individual half-wavelength dipoles. Chaff was released for exactly two minutes while the chaff release aircraft circled at 1.6 km above the surface within the dry convective boundary layer 15 km south of the radar. The aircraft track for this test is shown in Figure 5.1. Only one of the two cutters on board was used for this test and the total number of revolutions of the cutter wheel was counted during this time. Each revolution of the cutter wheel results in 20 cuts of the 3000 strand count chaff rope so that the total number of fibers cut during the two minute interval could be calculated from the following equation.

$$T = 89 \text{ rev/min} \times 2 \text{ min} \times 20 \text{ cuts/rev} \times 3000 \text{ fibers/cut}$$

This yields $T = 10.7 \times 10^6$ fibers. The observed number of fibers could be computed by first computing the chaff concentration from the measured reflectivity, and then integrating the concentration over the chaff cloud volume. That number is then divided by T to arrive at an efficiency estimate. Calculations for three radar volume scans are described below.

Reflectivity from randomly oriented chaff can be related to chaff concentration by the following relationship (Schlesinger, 1961):

$$Eta = 0.18 \times lambda^2 \times F \qquad (1)$$

where Eta is radar reflectivity or radar cross section per unit volume (units are m^{-1}), lambda is the radar wavelength (m) and F is the concentration of chaff fibers (fibers/km^3). The quantity routinely measured by the NOAA radars is equivalent reflectivity factor which can be expressed as:

$$Z_e = (Eta \times lambda^4) / (pi^5 \times K^2) \qquad (2)$$

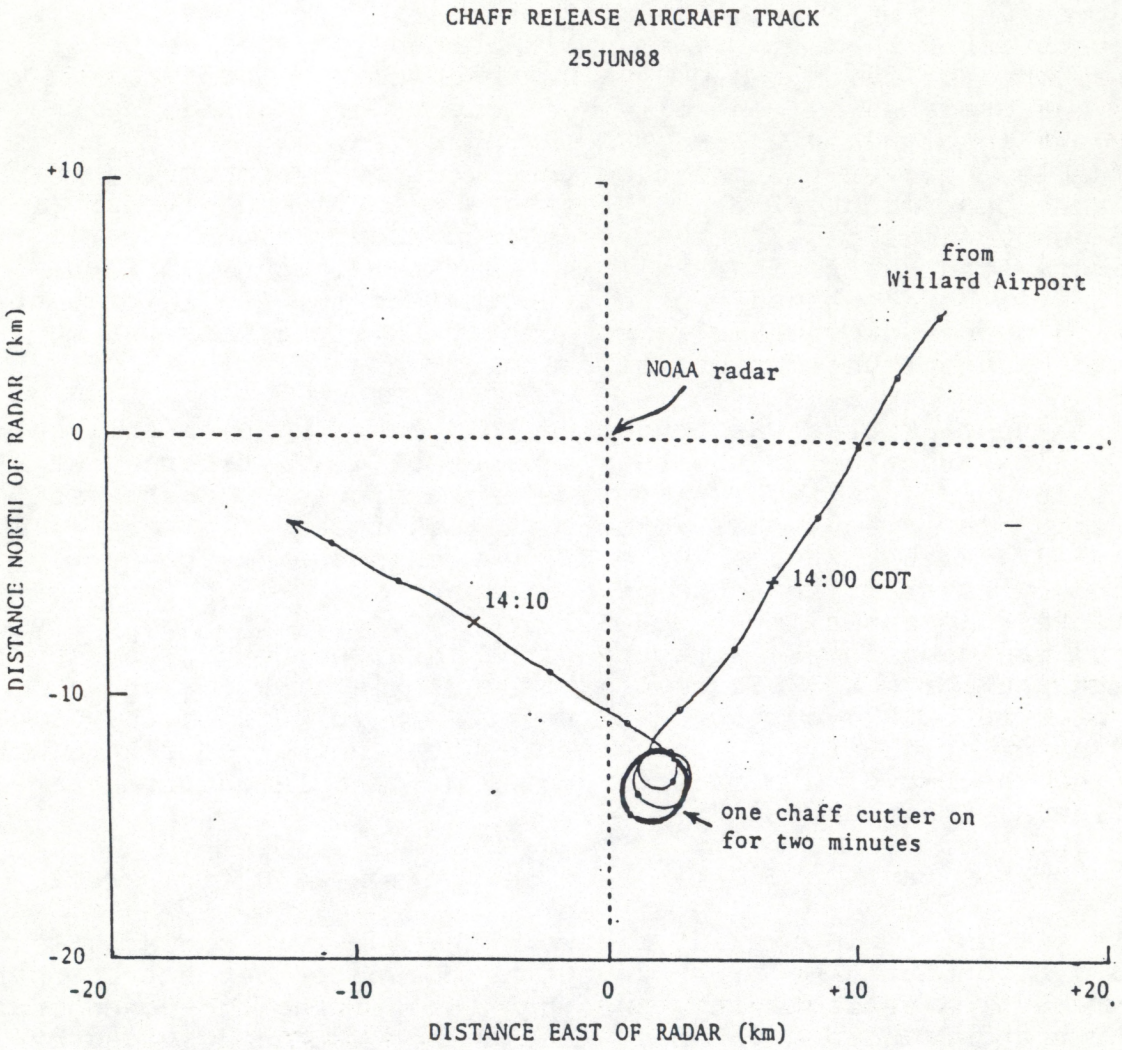

Figure 5.1. Track of the chaff release aircraft during the chaff cutter efficiency test on 25JUN88. The heavy line indicates where chaff was released for exactly two minutes. The aircraft flew at 1.6 km above the ground.

where Z_e is in m^3 units and K is the refractive constant for water (Battan, 1973).

Combining (1) and (2) for a 3.2 cm wavelength radar yields:

$$F = 1480 \times Z_e \qquad (3)$$

where the units of F are fibers/km^3 and Z_e is in traditional radar units of mm^6/m^3. In practice, the quantity dBZ = 10 log Z_e is recorded so that $F = \exp(7.3 + (0.23 \times dBZ))$ is the equation used for this test. By integrating F over the volume of chaff echo the total number of fibers, N, which were effectively scattering as individual dipoles is derived.

The radar measurements consisted of a series of 2.5 minute long volume scans through the chaff echo with nearly contiguous samples in azimuth, elevation and range. The measurements shown here were taken about 12, 15 and 18 minutes after the chaff was released, which is sufficiently long for the chaff to diffuse and fill the finite radar pulse volumes but not long enough for falling individual chaff fibers to reach the ground.

Figures 5.2 and 5.3 show horizontal cross-sections through the chaff cloud at 1.3 km above the ground about 12 minutes after the release and represent dBZ and F ($\times 10^{-4}$), respectively. Table 5.1 summarizes the overall results of the test with the measured concentrations averaged over the cloud, F-bar; the number of Cartesian grid cells (.15km x .15km x .15km) that contained echo from chaff, n; the total volume of chaff cloud, V; the observed effective number of fibers in the chaff cloud, N; and the estimated cutter efficiency, N/T, being shown as a function of time after release.

As expected, the average concentration is seen to decrease with time and the volume of the chaff cloud increases because of diffusion. The agreement between N for the samples at 15 and 18 minutes gives confidence in the corresponding efficiencies of 14.3% and 13.7%. Relatively large reflectivity gradients relative to the radar beam weighting function probably account for the lower value produced by the first sample. These gradients diminished with time because of turbulent diffusion. It appears that, under the conditions of this experiment, an efficiency of 14% is a representative baseline value for comparison with similar measurements after future chaff cutter modifications are implemented.

The vertical distribution of the amount of horizontally averaged chaff is shown in Figure 5.4. The total number of needles or area under the curves should remain constant in still air and the mean height should descend at the fall speed of chaff (0.3 m/s) while the distribution is broadened by turbulent diffusion with time. Some differences from these expectations are indicated in the figure. As discussed above, the first sample has only about .75 of integrated area of the later

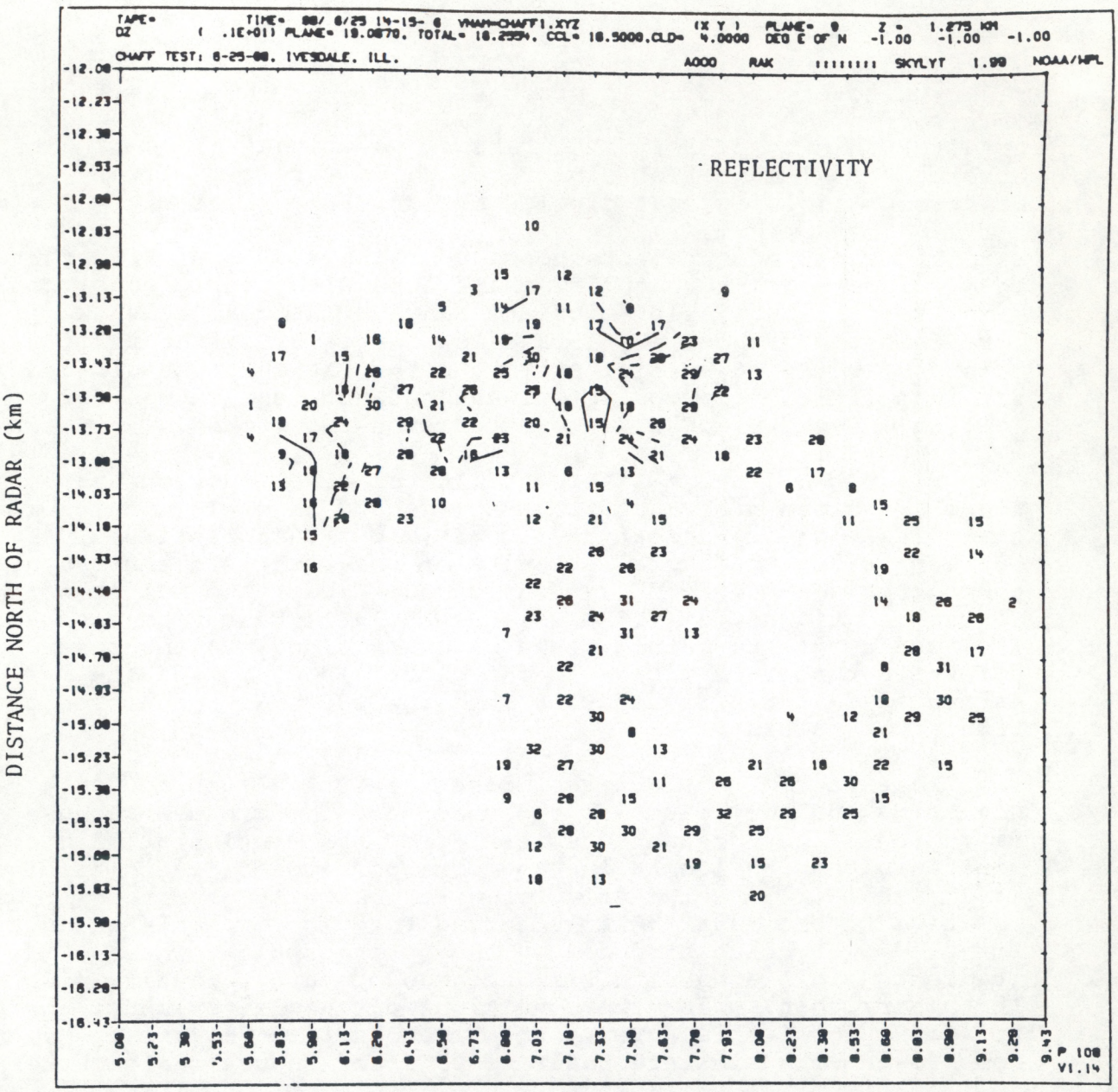

Figure 5.2. Reflectivity (dBZ) pattern measured by the NOAA X-band radar at 1.3 km above the ground 12 minutes after the chaff release on 25JUN88. The chaff had drifted about 6km east from the release point by this time.

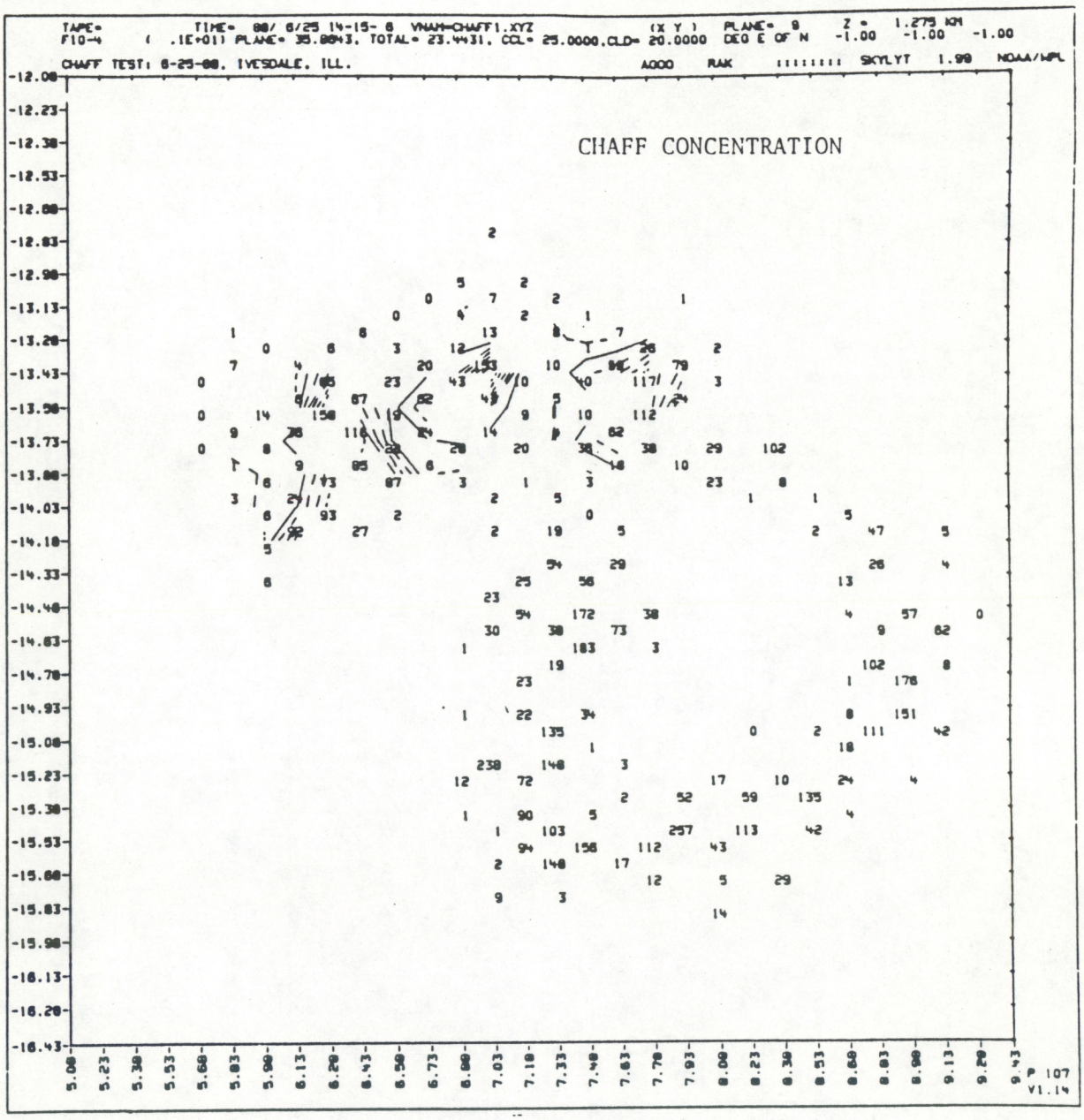

Figure 5.3. As in previous figure except the field shown is radar-derived concentration of chaff fibers, F ($x10^{-4}$), fibers/km^3.

Table 5.1
Summary of chaff cutter efficiency test
June 25, 1988

	Time after chaff release		
	12 minutes	15 minutes	18 minutes
F-bar (fibers/km^3)	23.4×10^4	20.3×10^4	15.8×10^4
n (# of cells)	1436	2237	2773
V (km^3)	4.85	7.54	9.34
N (millions of fibers)	1.14	1.53	1.47
N/T (%)	10.6	14.3	13.7

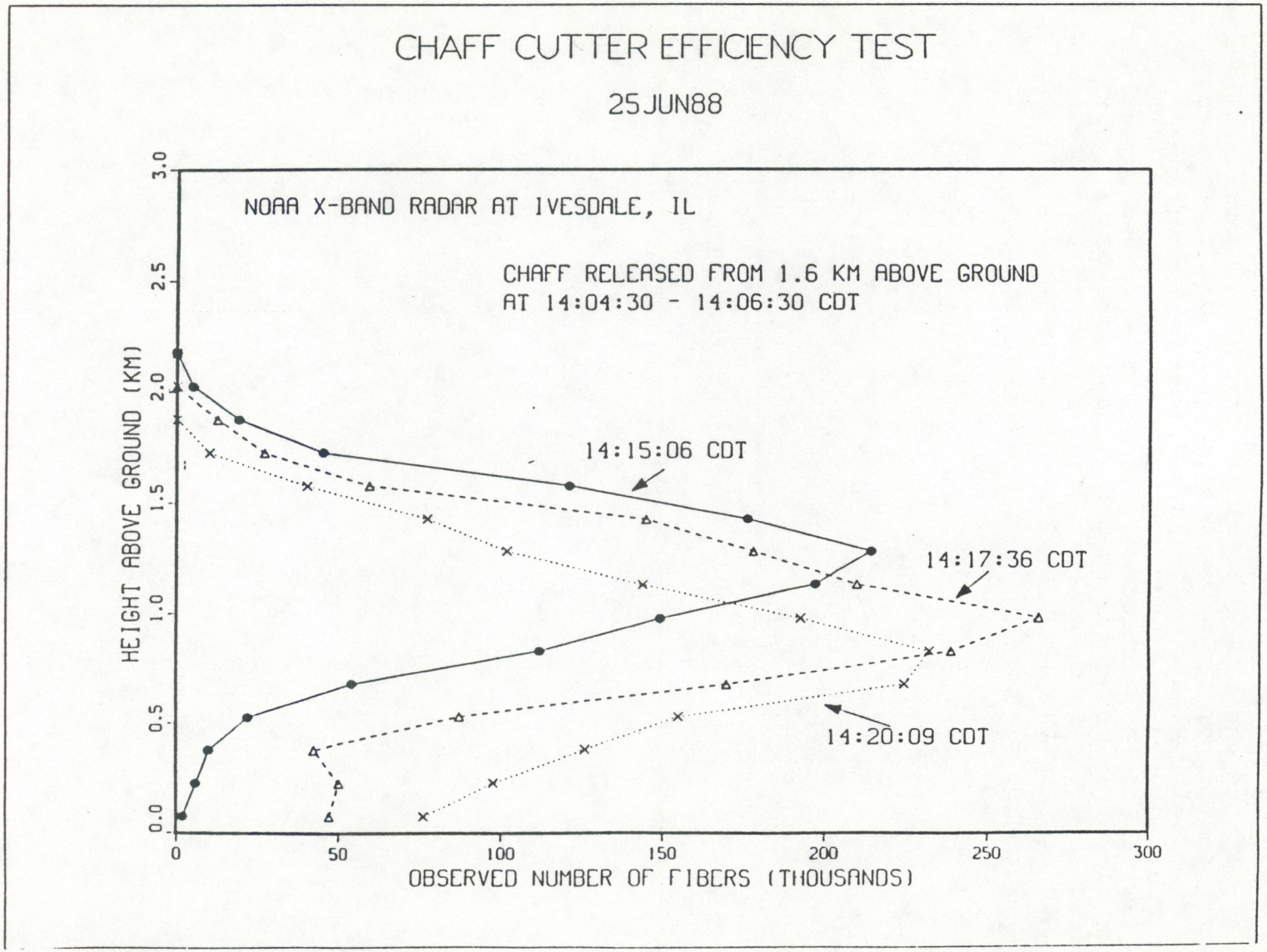

Figure 5.4. Vertical profiles of horizontally averaged number of chaff fibers observed by radar at three times after the chaff release.

samples. Also, the mean height appears to be falling faster than the fall speed of chaff, about 1 m/s if the last two samples are compared. Because the echo covered only about 4 to 7 km^2 which is similar to the size of typical convective thermal cells under these conditions, it is possible that the chaff was located preferentially within a downward branch of a convective circulation. In agreement with expectation, however, the half-width of the vertical distribution increased consistently with time from 750 m for the first sample to 800 m for the second, and to 850 m for the third. These small differences seem reasonable for the 2.5 minute time increments between samples.

6. Acknowledgments

Funding for the NOAA/WPL work in 3CPO was provided by the Electric Power Research Institute and was conducted under a subcontract to Battelle Pacific Northwest Laboratories. The authors wish to thank the following people at WPL: Bruce Bartram and Kurt Clark for their capable efforts in installing, maintaining and operating the NOAA X-band radar in Illinois, Steve Edwards for flying onboard the chaff release aircraft and operating the chaff cutters and airborne data system, and Eric Moore for data processing assistance. The NOAA Office of Aircraft Operations provided the Cessna 210 and installed the chaff cutters. The plane was piloted by Tom Gerish and Eric Secretan of the OAO. Lyle Lilie of Science Engineering Associates provided and installed the airborne data system. We are especially grateful to Dr. Jeremy Hales of Battelle Labs for his encouragement and enthusiastic support of our experiment.

7. References

Barnes, S.L., 1980: Report on a meeting to establish a common Doppler radar data exchange format. Bull. Amer. Meteor. Soc., 61, 1401-1404.

Battan, L.J., 1973: Radar Observation of the Atmosphere, Univ. Chicago Press, 324pp.

Browning, K.A., and R. Wexler, 1969: The determination of kinematic properties of a wind field using a Doppler radar. J. Appl. Meteor., 7, 105-113.

Businger, J.A., 1982: Equations and concepts, Atmospheric Turbulence and Air Pollution Modeling, F.T.M. Niewstadt and H. Van Dop, eds., D. Reidel, 456 pp.

Daum, P. 1988: 3CPO - Cloud Chemistry and Cloud Physics Organization Operational Plan, Brookhaven Natl. Lab, 112 pp.

Frisch, A.S. and S.F. Clifford, 1974: A study of convection capped by a stable layer using Doppler radar and acoustic echo sounder. J. Atmos. Sci., 31, 1622-1628.

Frisch, A.S. and R.G. Strauch, 1975: Doppler radar measurements of turbulent kinetic energy dissipation rates in a northeastern Colorado convective storm. J. Appl. Meteor., 15, 1014-1097.

Kaimal, J.C., J.C. Wyngaard, D.A. Haugen, O.R. Cote, Y. Izumi, S.J. Caughey and C.J. Readings, 1976: Turbulence structure in the convective boundary layer. J. Atmos. Sci., 33, 2152-2169.

Kropfli, R.A., 1986: Single Doppler radar measurement of turbulence profiles in the convective boundary layer. J. Atmos. Oceanic Technol., 3, 305-314. (reprint included in Appendix B)

Kropfli, R.A. and B. E. Martner, 1988: Meteorological applications for chaff and circular polarization diversity radar. Polarimetric Technol. Workshop, U.S. Army Redstone Arsenal, 10pp. (reprint is included in Appendix B)

Lenschow, D.H., J.C. Wyngaard and W.T. Pennell, 1980: Mean field and second moment budgets in a baroclinic convective boundary layer. J. Atmos. Sci., 37, 1313-1326.

Lhermitte, R.M., 1968: Turbulent air motion as observed by Doppler radar. Proc. 13th Conf. on Radar Meteor., Montreal, Amer. Meteor. Soc., 498-503.

Misra, P.K., 1982: Dispersion of non-buoyant particles inside a convective boundary layer. Atmos. Environ., 16, 239-243.

Moninger, W.R. and R.A. Kropfli, 1987: A technique to measure entrainment in cloud by dual-polarization radar and chaff. J. Atmos and Oceanic Technol., 36, 75-83.

Schlesinger, R.J., 1961: Principles of Electronic Warfare, Prentice-Hall, 213pp.

Sisterson, D.L., 1987: 3CPO - Cloud Chemistry Cloud Physics Organization Coordination Document. Argonne Natl. Lab, 138 pp.

Wilson, D.A., 1970: Doppler radar studies of boundary layer wind profiles and turbulence in snow conditions. Proc. 14th Conf. on Radar Meteor., Tucson, Amer. Meteor. Soc., 191-196.

APPENDIX A

****

NOAA/C X-BAND RADAR

FIELD DATA TAPE LOG FOR 3CPO PROJECT

****

TAPE	DATE	TIME (CDT)	COMMENTS
001	2JUN88	1337-1356	Small convective cells, no chaff
002	"	1356-1645	"
003	"	1647-1727	"
004	"	1728-1743	"
005	3JUN88	1630-1637	Ground clutter pattern
006	"	1644-1936	Chaff test flight
007	"	1937-1949	"
008	6JUN88	0906-0924	Clear air VAD scans
009	"	0925-0942	"
010	"	0943-1001	"
011	"	1002-1019	"
012	"	1020-1145	"
013	"	1146-1311	"
014	"	1312-1433	"
015	"	1434-1552	"
016	"	1900-0350	Clear air vertical scans
017	7JUN88	0427-1132	"
018	"	1133-1509	"
019	"	1539-1555	Chaff test flight
020	"	1555-1613	"
021	"	1614-1633	"
022	"	1635-1657	"
023	"	1658-1715	"
024	8JUN88	1458-1514	Chaff in widespread stratus rain
025	"	1514-1530	"
026	"	1531-1547	"
027	"	1548-1604	"
028	"	1605-1623	"
029	"	1623-1637	"
030	"	1640-1736	"
031	9JUN88	1345-1407	Chaff test flight
032	"	1408-1426	"
033	10JUN88	1340-1353	Calibrations
034	11JUN88	1900-2344	Clear air vertical scans
035	11JUN88	2345-0400	"
036	12JUN88	0939-1039	Clear air VAD scans
037	"	1109-1238	"
038	"	1239-1404	"
039	"	1405-1522	"
040	"	1523-1639	"

TAPE	DATE	TIME(CDT)	COMMENTS
041	12JUN88	1900-0427	Clear air vertical scans
042	13JUN88	0428-0908	"
043	"	1409-1424	Chaff test flight
044	"	1425-1439	"
045	14JUN88	0951-1435	Clear air vertical scans
046	"	1436-1621	"
047	15JUN88	1414-1427	Chaff beneath very weak cumuli
048	"	1429-1449	"
049	"	1449-1506	"
050	"	1506-1523	"
051	"	1830-1848	"
052	"	1848-1903	"
053	"	1903-1920	"
054	"	1920-1938	"
055	"	1939-1956	"
056	"	1957-2008	"
057	17JUN88	1328-1343	Chaff diffusion test in clear air
058	"	1344-1402	"
059	"	1403-1421	"
060	"	1422-1555	"
061	18JUN88	0926-1853	Clear air vertical scans
062	"	1854-0421	"
063	19JUN88	0422-0918	"
064	"	1014-1145	Clear air triple angle VAD scans
065	"	1146-1318	"
066	"	1318-1449	"
067	"	1450-1621	"
068	23JUN88	1900-0432	Clear air nocturnal vertical scans
069	24JUN88	0433-0908	"
070	"	1701-1740	Chaff beneath very weak cumuli
071	"	1741-1800	"
072	"	1800-1803	"
073	25JUN88	1405-1448	Chaff test flight
074	"	1448-1523	"
075	"	1524-1621	Time series data on chaff/clear air
076	29JUN88	0802-1045	Chaff in virga/midlevel stratus
077	"	1046-1101	"
078	"	1519-1533	"
079	1JUL88	1003-1413	Clear air triple angle VAD scans
080	"	1414-1452	"
081	"	1509-1655	Time series in clear air & chaff

Universal format tapes have same numbers with suffix "U".
Field tapes and universal format tapes are archived at NOAA/WPL.

Example of daily log notes recorded by the NOAA X-band radar crew on computerized METALOG system. Notes are archived on floppy disk at NOAA/WPL and the 3CPO Data Management Office.

**** Log entries for C3PO Experiment. Starting at
1201 Wednesday 22-June-1988

At the NOAA Radar: Brooks Martner and Bruce Bartram.

**** WEATHER:
1201 Wednesday 22-June-1988
Broken cirrus, hazy, hot and windy. There is a line of showers stretching from Milwaukee to Des Moines which is slowly moving our way ahead of a cold front. Howvever, the atmosphere is very dry over Illinois so the project forecasters hold little hope for today.

The front may pass tonight.

**** WEATHER:
1205 Wednesday 22-June-1988
Surface winds are from the SW at 15 mph and record-breaking temperatures are expected here again today.

**** EXPERIMENTAL EVENT:
1206 Wednesday 22-June-1988
The aircraft are scheduled for takeoffs at 3:30. Bruce has the radar temporarily down while he works on some software changes.

**** WEATHER:
1309 Wednesday 22-June-1988
Cirrus overcast now; still windy.

**** WEATHER:
1432 Wednesday 22-June-1988
Sun dimly visible through the cirrus overcast. CHILL and Springfield radars report weak echoes beyond our range.

**** EXPERIMENTAL EVENT:
1434 Wednesday 22-June-1988
We have turned the radar on for a few minutes to take a look. Nothing out there. Bruce will resume software work.

**** EXPERIMENTAL EVENT:
1520 Wednesday 22-June-1988
We have postponed the Cessna's takeoff to 4:30 at the earliest.

**** EXPERIMENTAL EVENT:
1531 Wednesday 22-June-1988
The P3 has taken off for a clear air boundary layer flight. Transponder code is 1352.

EXAMPLE OF FLIGHT TRACKS PRODUCED FROM CHAFF RELEASE AIRCRAFT DATA SYSTEM

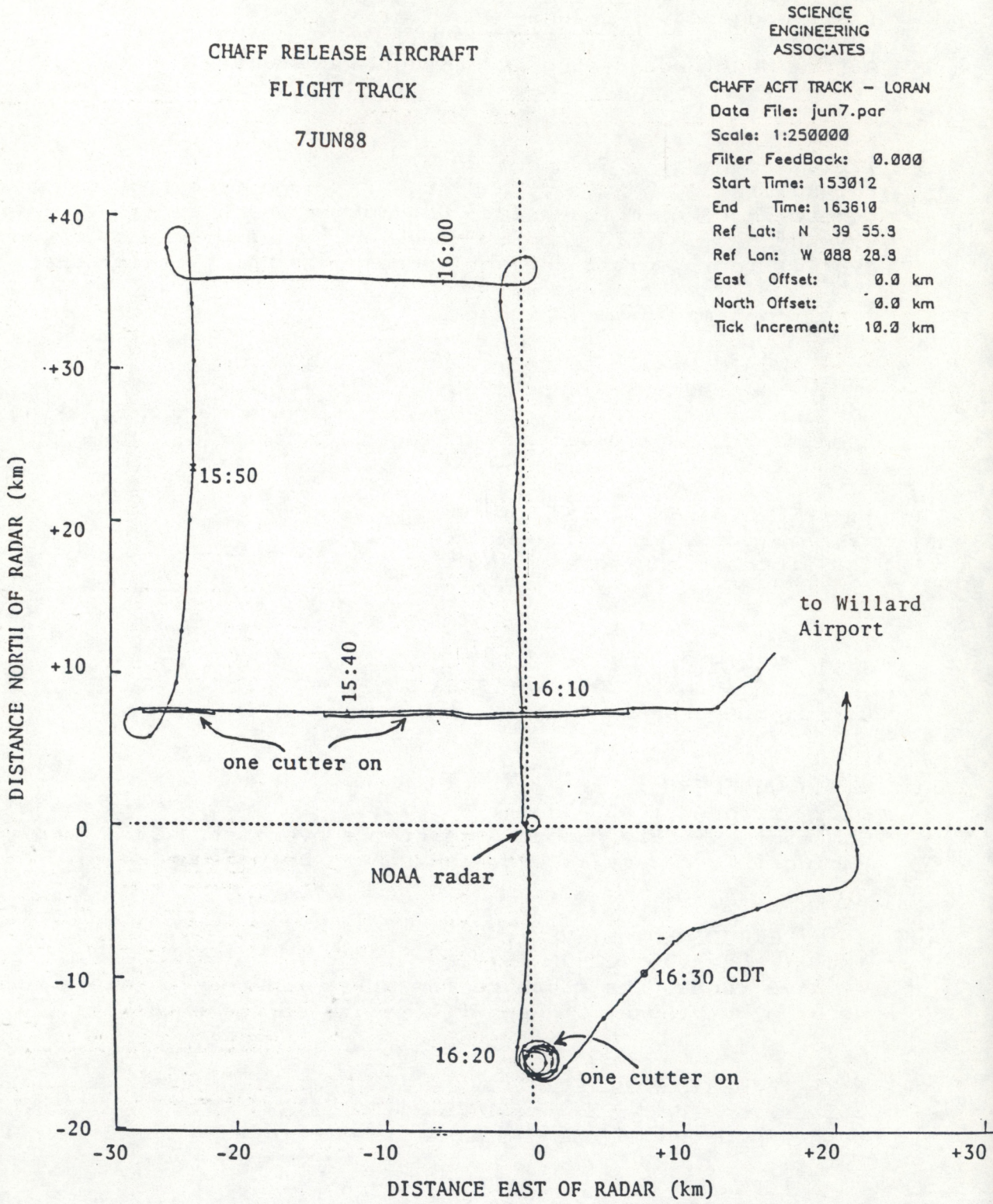

The News-Gazette

136th Year No. 335 ★ ★ Champaign-Urbana — Friday, July 1, 1988 — 54 Pages Daily 35 Cent

Area sets series of records for dryness

By STEVE BAUER
News-Gazette Staff Writer

Crops and soil are showing more signs of stress as the area has set records for the driest June ever, the driest growing season ever and the driest January-to-June in nearly 100 years.

By June 15, there was zero moisture available at the 6-inch soil level statewide, according to the Illinois State Water Survey. Area crops are getting most of their water from the area down to 20 inches below the surface and even that is drying out.

Ag officials look for unjustified food price increases, B-6.

"Even as far down as 20 inches, almost 2 feet, we are running out of water," said Steven Hollinger, Illinois State Water meteorologist and agronomist. "For all practical purposes, there's no water available on the top."

There's still plenty of moisture available below 20 inches, but not many corn roots can reach that far down, Hollinger said. And as the deep soils are drying out, the soil will hold onto the water with greater tension than the plants can pull it out.

There's been no rain in Champaign-Urbana since .32 inch fell on June 8 — the only measurable rainfall in the month — and none is expected in the foreseeable future.

Water survey records show:

- Only 3.37 inches of precipitation fell in Champaign-Urbana from April through June, breaking the previous record for driest growing season of 4.35 inches in 1925.
- The .32 inch of rain in June made for the driest June ever, breaking the old mark of .44 set in the Dust Bowl year of 1936.
- And the 9.33 inches of precipitation during the past six months made 1988 the driest January-to-June since only 9.44 inches fell in 1895.

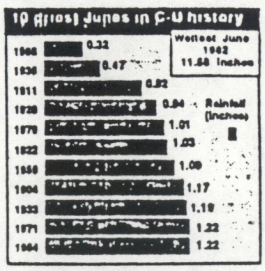

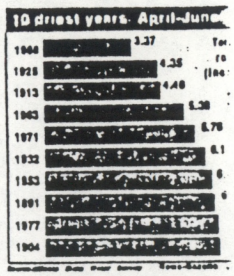

The driest month ever in Champaign-Urbana was November 1903 when just a trace of precipitation was reported.

Not only was June dry. It was hot. Wayne Wendland, a meteorologist with the water survey, June average daily temperat statewide were 6 to 10 deg above the average.

(See DRYNESS, A-12)

Dryness

(Continued from A-1)

"And the average high temperatures across the state are going to be 9 to 10 degrees above the average," Wendland said. "That's a lot."

In Champaign-Urbana, there were 16 days in June in which temperatures hit 90 degrees or more. That is 10 days above average. The highest reading was 103 degrees on June 25.

Two large areas of the state had less than a half-inch of rain in June, Wendland said. One area was south of a line from Carbondale to Harrisburg and the other was 50 miles on either side of a line from Freeport to Champaign.

In other central Illinois communities, Danville and Bloomington both recorded .31 inch for June. Springfield had .62 inch, Decatur had .64 inch and Charleston .71 inch — all well below normal.

Locally, the .32 inch June precipitation was about 8 percent of the normal 3.92 inches. Statewide, precipitation was 25 to 30 percent below the June average of 4 inches, Wendland said.

"IN MANY CASES, we're in uncharted territory," Hollinger said. "Nobody has ever observed this type of spring and summer."

The parched April-June season has had a significant impact on reducing area corn and soybean yields, already reducing estimated corn yields by 25 to 30 percent.

"We would have to have above average July and August rainfall to even approach normal," Hollinger said. "For all likelihood, the growing season will be drier than normal."

But the National Weather Service this week issued a drought advisory predicting that precipitation will be below normal and temperatures above the norm for July.

And the forecast for the next 10 days — probably more reliable — calls for persistent hot, dry weather.

"No precipitation is expected through the next five days," said Fred Snowden, meteorologist with the National Weather Service in Springfield. "The forecast for July 5-9 is for above normal temperatures and below normal precipitation."

THAT COULD BE the real problem for area corn that will be going through the critical tassel and pollination stages.

"If we were to get an inch and a half to 2 inches of rain in the next seven days, that would go a long way toward mitigating the effects of the drought," Hollinger said.

Hollinger said there's still time for rain to help area crops, particularly soybeans. But time is critical.

"Each day we go without rain, we're in a deteriorating situation," Hollinger said. "Each day we get rain, it makes our prospect look better."

The crops can go either way, according to John Unger, crop statistician for the Illinois Agricultural Statistical Service.

"As far as corn and soybeans, the verdict is still out," Unger said. "Most of the corn acreage around the state is still in a position that it could respond to rainfall."

Unger said temperature might be just as important as precipitation to pollination and tasseling.

"During the coming two-week period, precipitation will help that process," Unger said. "If temperatures would stay below 90 degrees, it would be even better."

THE LAST TWO YEARS, like this year, also were early crop years, Unger said.

The average corn yield for Champaign County in 1987 was 154 bushels per acre, compared with the statewide yield of 132 bushels. The 1987 spring growing season of April to June had 11.5 inches of precipitation, with 7.8 inches in the July tassel period.

In 1986, the average yield in the county was 144 bushels per acre, compared with the statewide average of 135 bushels. Total precipitation for April-June that year was 9.67 inches, with another 4.7 inches in July.

In 1983, however, there was a super-abundance of rain in April-June —, more than 21 inches. But it was dry in July with only 1.4 inches and average yields that year dropped to 89 bushels in Champaign County and 79 bushels in the state.

"The corn didn't pollinate," Unger said. "There were no ears on much of that corn."

APPENDIX B

REPRINTS OF PERTINENT ARTICLES

POLARIMETRIC TECHNOLOGY WORKSHOP
16 - 18 August 1988
Redstone Arsenal, Alabama, U.S.A.

METEOROLOGICAL APPLICATIONS FOR CHAFF AND CIRCULAR POLARIZATION DIVERSITY RADAR

Robert A. Kropfli and Brooks E. Martner

NOAA/ERL/Wave Propagation Laboratory
Boulder, Colorado

1. INTRODUCTION

Radars with polarization diversity capability can provide atmospheric scientists with useful information about the shape and orientation of hydrometeors. Research has been conducted in this area for almost two decades. In this article we describe a new technique which utilizes special capabilities of circular polarization diversity radar to detect and measure certain characteristics of chaff fibers which serve as tracers of airflow when released in the atmosphere. The technique allows the radar to map the trajectory of a chaff-filled parcel of air as it moves from clear air into and through clouds. This has not been possible before, not even with linear polarization diversity radars. The technique and other unique features of the interaction of circularly polarized waves with chaff are potentially valuable for investigating a number of basic questions about clouds.

The exchange processes which occur at cloud boundaries are important but poorly understood aspects of storm dynamics, precipitation processes, atmospheric chemistry and cloud electrification. Entrainment of unsaturated environmental air is a crucial factor in limiting cloud longevity and, thus, precipitation development. Dry air entrained through the sides or top of a convective cloud can greatly influence the storm's microphysics as well as its dynamics. Tropospheric pollutants may be transported out of the boundary layer by tall cumulus turrets into the stratosphere where they are potentially more disruptive to climate balances. Less vigorous cumulus clouds can transport these pollutants to the upper levels of the troposphere where they can be transported over long distances, eventually being deposited at the surface as acid rain many hundreds of kilometers from their sources.

Unfortunately, progress in understanding these problems has been slow because of the lack of good techniques to detect and follow the movement of air parcels

from the clear air into and through clouds. Methods that have shed some light on the entrainment process include in-situ and remote sensing measurements (Reuter, 1986)[1]. The in-situ techniques involve cloud penetrations by aircraft equipped to measure air parcel properties that are conserved in cloud processes such as equivalent potential temperature and total water content (Paluch, 1979[2]; Boatman and Auer, 1983[3]) or to detect tracer chemicals such as sulfur hexafluoride emitted by another aircraft (Stith et al., 1986[4]) or to sample atmospheric trace chemicals that in normal circumstances are distributed in steady and known concentrations in the vertical through the cloud-free atmosphere (Dickerson et al., 1987[5]). In addition to individual weaknesses, each of the aircraft techniques suffers from the inherent fact that the aircraft samples only along a line, and the larger scale picture of motions must be inferred from evidence based on sampling a tiny fraction of the whole cloud volume.

A new radar technique proposed by Moninger and Kropfli (1987[6]) offers a promising approach for studies of both environmental entrainment by clouds and the relatively small-scale motions within clouds. The technique calls for the use of a radar that can detect depolarized signals backscattered by chaff targets. The circular depolarization ratio (CDR) from chaff is measured by the radar and provides a signal that stands out very strongly in clear air, but unlike reflectivity, also maintains a clear signature within cloud. The CDR-chaff tracer technique, also known as TRACIR (TRacking Air with CIrcular-polarized Radar), forms the basis for the discussion that follows.

2. THE CDR - CHAFF TRACER TECHNIQUE (TRACIR)

Although the reflectivity of chaff has been widely used as a tracer of air motions outside cloud, its strong depolarizing signature has been overlooked until very recently. Dual-polarization techniques offer an opportunity to follow chaff as it moves through a cloud. Because chaff and natural hydrometeors have significantly different polarization properties, the chaff signal can be readily distinguished from the cloud signal.

---

[1]Reuter, G.W., 1986: A historical review of cumulus entrainment studies. Bull. Amer. Meteor. Soc., 67, 151-155.

[2]Paluch, I.R., 1979: The entrainment mechanism in Colorado cumuli. J. Atmos. Sci., 36, 2467-2478.

[3]Boatman, J.F., and A.H. Auer, Jr., 1983: The role of cloud top entrainment in cumulus clouds. J. Atmos. Sci., 40, 1517-1534.

[4]Stith, J.L., D.A. Griffith, R.L. Rose, J.A. Flueck, J.R. Miller, Jr., and P.L. Smith, 1986: Aircraft observations of transport and diffusion in cumulus clouds. J. Climate & Appl. Meteor., 25, 1959-1970.

[5]Dickerson, R.R., G.J. Huffman, W.T. Luke, L.J. Nunnermacker, K.E. Pickering, A.C.D. Leslie, C.G. Lindsey, W.G.N. Slinn, T.J. Kelly, P.H. Daum, A.C. Delaney, J.P. Greenberg, P.R. Zimmerman, J.F. Boatman, and D.H. Stedman, 1987: Thunderstorms: an important mechanism in the transport of air pollutants. Science, 235, 460-465.

[6]Moninger, W.R., and R.A. Kropfli, 1987: A technique to measure entrainment in cloud by dual-polarization radar and chaff. J. Atmos. & Ocean. Techn., 4, 75-83.

Nonspherical objects depolarize incident microwaves (some energy is scattered with its electric field vector orthogonal to the field of the incident transmitted wave) whereas spherical targets do not. Atmospheric scientists have used this fact with some success in attempts to distinguish between hydrometeors of different shapes in clouds. This research has included efforts at hailstone (irregular shapes) detection (e.g., Barge, 1972[7]; Bringi et al., 1986a[8]) and efforts to delineate regions of ice particles (highly nonspherical), raindrops (oblate spheroids), and cloud droplets (almost perfectly spherical) within storms (Kropfli et al., 1984[9]; Bringi et al., 1986b[10]). Most of the more recent studies have used linearly polarized radars, but we shall show that circular polarization is better suited to detecting chaff fibers (extremely nonspherical) in clouds.

Radar-reflective chaff consists of 25-micron diameter aluminum-coated glass filaments, cut to a length equal to one-half the radar wavelength so they are resonant dipole targets. The terminal fall speed of the filaments is about 0.3 m/s in still air, which is at least an order of magnitude less than typical vertical motions within convective clouds. Thus, the chaff can be assumed to drift essentially with the air, and its path closely approximates the trajectory of the air parcel within which it resides. The reflectivity of chaff is determined by the number density of filaments that constitute the scattering volume and by the radar wavelength. Numerous earlier experiments using the NOAA/Wave Propagation Laboratory X-band (3 cm wavelength) radars have demonstrated the radars' ability to detect useful concentrations of chaff in clear air at ranges up to 60 km. The chaff is usually released from an airplane carrying a chaff-cutting device, which produces from one to five million filaments per minute. Experience shows that only about 10% of the chaff falls as individual filaments, but this is sufficient for easy detection of the chaff's reflectivity signal in clear air. The remaining 90% falls out as clumps and clusters of filaments.

Although it is a simple matter to detect chaff in clear air by its reflectivity, distinguishing the chaff inside a cloud depends on the use of polarization techniques. Consider a radar that transmits, say, left-hand (LH) circular polarized radiation. If the signal is reflected back to the radar from spherical targets, the polarization properties of the radiation remain unchanged, but the propagation direction is reversed; hence, the transmitted LH radiation becomes

---

[7]Barge, B.L., 1972: Hail detection with polarization diversity radar. Sci. Rep. MW-71, Stormy Weather Group, McGill University, 80 pp.

[8]Bringi, V.N., J. Vivekanandan and J.D. Tuttle, 1986a: Multiparameter radar measurements in Colorado convective storms. Part II: Hail detection studies. J. Atmos Sci., 43, 2564-2577.

[9]Kropfli, R.A., W.R. Moninger, and F. Pasqualucci, 1984: Circular depolarization ratio and Doppler velocity measurements with a 35-GHz radar during the Cooperative Convective Precipitation Experiment. Radio Sci., 19, 141-147.

[10]Bringi, V.N., R.M. Rasmussen and J. Vivekanandan, 1986b: Multiparameter radar measurements in Colorado convective storms. Part I: Graupel melting studies. J. Atmos. Sci., 43, 2545-2563.

right-hand (RH) circular. Thus, the RH receiver channel is called the main channel, and the power received in the main channel is P_m. As a result of the depolarization caused by deformities in the scattering particles, some of the returned radiation is received in the LH channel (the cross channel); the power received in the cross channel is P_c. A measure of the depolarization of the signal, the circular depolarization ratio (CDR), is given by

$$CDR = 10 \log(P_c / P_m). \quad (1)$$

For cloud droplets, CDR is less than -25 dB (Hendry et al., 1976[1]). For ice and raindrops, CDR is in the range -25 dB to -15 dB. For large melting snowflakes, such as those found just below the 0°C level in precipitating clouds, CDR is -10 dB to -5 dB. Only rarely (as for hail) does CDR exceed -5 dB for natural hydrometeors. For clouds in their early stages of growth, CDR should generally be less than -20 dB.

The backscattered signal from a resonant dipole such as chaff is linearly polarized along the direction of the dipole. Since linear polarization can be vectorially decomposed into RH and LH components having equal amplitude, the CDR for chaff should be 0 dB, regardless of the orientation of the dipole. Our observations (see below) have confirmed this expectation. Thus we would expect at least a 20-dB difference between the polarization signatures of chaff and cloud particles.

To quantify this further, we note that when the cloud hydrometeors and chaff are mixed, the resulting CDR is

$$CDR(chaff+cloud) = 10 \log((P_{cc} + P_{ch})/(P_{mc} + P_{mh})), \quad (2)$$

where P_{cc} and P_{ch} are the echo power in the cross channel provided separately by the chaff and the hydrometeors, and P_{mc} and P_{mh} are the echo power in the main channel from the chaff and the hydrometeors. Since we know that $P_{cc} = P_{mc}$, and if we define the hydrometeor to chaff received-power ratio as $R = P_{mh}/P_{mc}$ and $CDR(cloud) = 10\log(f)$ where $f = P_{ch}/P_{mh}$, we can write

$$CDR(chaff+cloud) = 10 \log((1+fR)/(1+R)). \quad (3)$$

For the usual method of chaff detection, which employs only measurements of reflectivity, we assume that we can no longer reliably distinguish chaff from the cloud background when the signature of the mix of chaff and hydrometeors is less than 3 dB above the cloud background. This 3 dB threshold occurs at $R=1$ (i.e., $P_{mc} = P_{mh}$) when main channel signal power alone is used to identify chaff from the background cloud.

---

[1]Hendry, A., G.C. McCormick, and B.L. Barge, 1976: The degree of common orientation of hydrometeors observed by polarization diversity radars. J. Appl. Meteor., 15, 633-640.

To determine an equivalent threshold $R = R_t$ for the polarization technique that exploits CDR rather than reflectivity, we require the same detection criterion, i.e., CDR(chaff+cloud) - CDR(cloud) = 3 dB which reduces to

$$R_t = (1/f) - 2. \tag{4}$$

In typical clouds for which $f<0.01$, Eq.(4) yields $R_t > 100$, which indicates a 20-dB improvement over the conventional reflectivity technique. Even with exceptionally strongly depolarizing hydrometeors (e.g., $f=0.1$), it would be possible to detect chaff signals about 8 times weaker than the conventional method that uses only echo power.

The CDR signature does not depend on the aggregate orientation of the chaff; it will be the same whether the chaff is randomly or uniformly oriented. A different but commonly used polarization technique involving linear polarization measures differential reflectivity, Z_{DR}, which is given by

$$Z_{DR} = 10 \log(P_H/P_V), \tag{5}$$

where P_H is the power received at horizontal polarization and P_V is the power received at vertical polarization. The Z_{DR} technique for identifying chaff is inferior to the CDR technique because Z_{DR} will vary depending on the aggregate chaff orientation. Thus, if chaff filaments are randomly oriented, as might occur, for instance, in the turbulent portions of a convective cloud, the Z_{DR} signature of the chaff will be zero because $P_H = P_V$. However, if chaff is falling with a preferred orientation (as it does in still air) P_H and P_V differ greatly, resulting in a quite different Z_{DR} value. A number of atmospheric research radars are capable of measuring Z_{DR}, but the NOAA Wave Propagation Laboratory has the only meteorological research radars in the United States that use circular polarization and can measure CDR. These radars operate at K_a-band (8.6 mm) and X-band (3.2 cm) wavelengths.

3. TECHNIQUE VERIFICATION

The first task in verifying that the method works as predicted is to measure the circular depolarization ratio in clear air. To this end, chaff was released from an aircraft into clear air on January 10, 1985. Figure 1 shows the CDR values of this chaff observed from a distance of 10 km with the NOAA K_a-band radar. The 213 data points show a mean CDR of 1.3 dB, with a standard deviation of 0.9 dB. We believe the slight positive value of the mean CDR, as opposed to the expected value of 0 dB, is the result of slight relative calibration errors between the main and cross-polarized channels. The mean CDR obtained from more recent experiments indicates a mean value of about .2 dB. In any case, the CDR of chaff alone is well above the measured CDR of natural hydrometeors.

The second task is to show that chaff can be seen in regions of space having substantial reflectivity from natural hydrometeors. On August 1, 1985, we conducted our first experimental study of this with the same K_a-band radar. On this day, bases of the small-to-moderate cumulus clouds were at 4.3 km above the

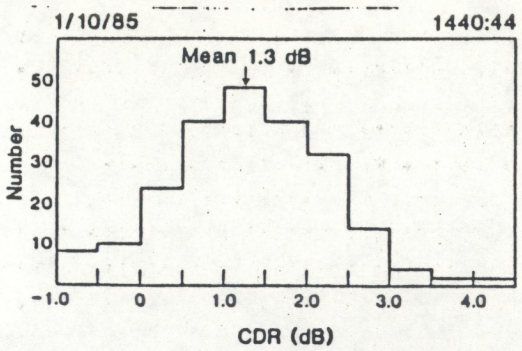

Figure 1. Histogram of circular depolarization ratio values from the NOAA K_a-band radar for chaff release into clear air on 10 Jan 1985.

ground, and the amounts of virga descending below this level were substantial. Because of the air traffic and altitude limitations, the chaff-release airplane did not fly within the cloud. However, the virga did provide substantial radar reflectivity without restricting visibility from the aircraft. The airplane flew on a north-south line, east of the radar at 1.9 km above ground.

Figure 2 shows reflectivity and CDR in the virga shaft as a function of range from the radar along an azimuth nearly perpendicular to the airplane's path approximately 10 minutes after the chaff was released. It shows that the airplane had flown in a region of rain having a reflectivity of 4 to 11 dBZ. The CDR plot shows a prominent peak at a range of 8.5 km, which was also the aircraft's distance from the radar. This peak of CDR is the chaff signature. As expected, however, the reflectivity data give no indication of the chaff's presence because the reflectivity of the raindrops obscured the chaff's reflectivity. Additional examples of the CDR-chaff signature on this day are given by Moninger and Kropfli (1987). This example illustrates that the chaff CDR signal can be detected within reflectivities

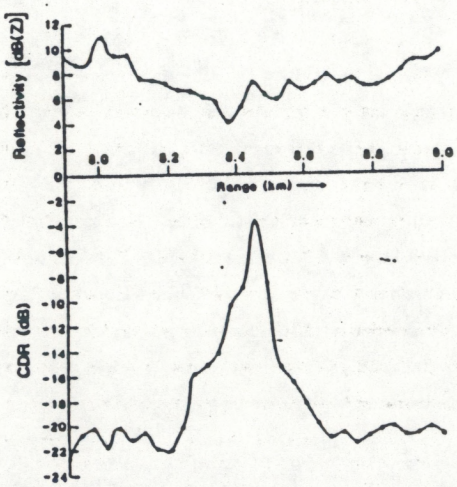

Figure 2. Reflectivity (upper) and CDR (lower) from the NOAA K_a-band radar on 1 Aug 1985 along an azimuth nearly perpendicular to the path of the aircraft as it released chaff in a light rain shower.

typical of weakly precipitating convective clouds. For examples in more intense thunderstorms we turn to data collected in the 1987 CINDE project.

On July 28, 1987 the NOAA X-band radar scanned a thunderstorm that was penetrated at middle levels by the University of Wyoming King Air, which was equipped with a NOAA chaff cutter. The aircraft location was measured to great precision by a combination of LORAN, Inertial Navigation System, and VOR-DME positioning instruments onboard. At the time of the penetrations, part of the storm had already reached 40 dBZ, and it continued to intensify rapidly.

Perspective views of the resulting data are shown in Figure 3 for the aircraft track, reflectivity, and CDR. Chaff is detectable in thin lines of 15 dBZ on the western side of the cloud in the reflectivity display (Fig. 3b), but the chaff signal is totally lost within the storm's reflectivity. The track of the chaff does appear prominently, however, in the radar's CDR signal (Fig. 3c). The older, west-bound leg shows a wider region of chaff along the track as the chaff had some time to diffuse and drift. The newer, northeast-bound leg shows a very strong narrow chaff signal.

The CDR signal did not detect the chaff through the heart of the storm where the hydrometeor reflectivity exceeded 35 dBZ. This problem can be solved if greater concentrations (faster cutting rates) of chaff can be produced by the release aircraft. Cutters used by the military chop multiple spools of chaff simultaneously and produce chaff concentrations more than an order of magnitude greater than has been achieved with any of the NOAA devices.

The question of how strong the storm reflectivity must be to obscure the chaff CDR signal is currently being assessed by examination of additional data from the summer of 1987. We have also used an analytical approach. Although CDR of chaff is zero in clear air, it is less than zero inside cloud because the "chaffy" region is diluted with hydrometeors, which have a much lower CDR. Thus, the resulting CDR of the chaff-hydrometeor mixture lies somewhere in between and depends on the inherent CDR and relative concentrations of the two constituents. By solving the CDR equation for a mixture of chaff and hydrometeors (Eq. 2) with given background levels of reflectivity and CDR for hydrometeors alone, we have determined the reflectivity (and hence concentration) of chaff that is required to achieve a desired increase of the CDR signal of the mixture above the background. A graphical presentation of the solution is shown in Figure 4 for the case where the hydrometeors produce a background CDR of -20 dB (typical of rain) and a background reflectivity ranging from 0 to 40 dBZ. If the background reflectivity is 30 dBZ, for example, then according to Figure 4 only 10 dBZ from chaff will be required to produce a factor-of-2 increase of the chaff-hydrometeor mixture's CDR over the -20 dB background. Armed with these solutions, we now know the amount of chaff needed to produce a detectable signal through various cloud conditions.

Although some further development is desirable, the tests conducted to date certainly show that the CDR-chaff tracer technique has worked at least in weakly precipitating and nonprecipitating convective clouds. It will also work in intense

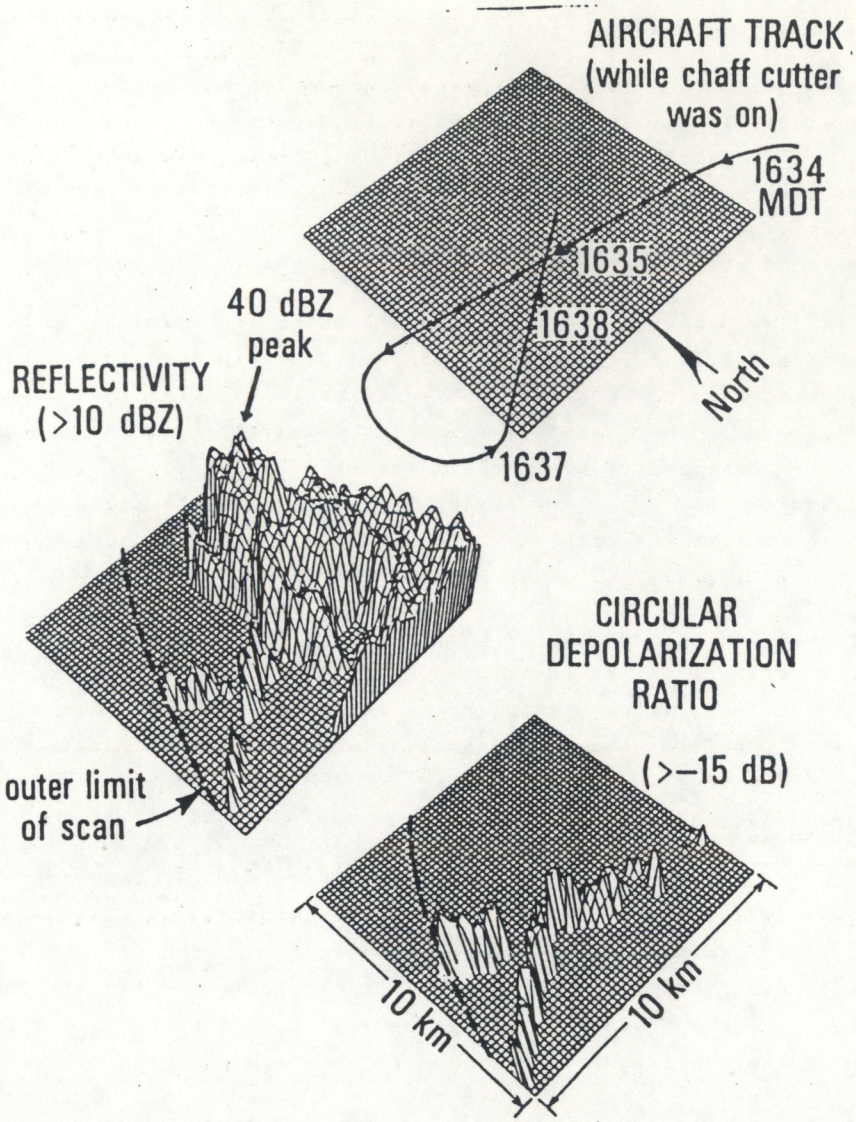

Figure 3. Perspective views of indicated quantities at 5.3 km MSL.

precipitation if we use faster (higher density) chaff cutters. This knowledge gives us confidence to apply the technique to a variety of atmospheric problems such as boundary layer venting by convective clouds and the lateral or cloud-top entrainment of environmental air into clouds.

4. ELECTRIC FIELD MEASUREMENTS

The electric field is another important cloud property that may be studied with chaff and dual (circular) polarization radar. In still air with no electric field, chaff filaments fall horizontally under the influence of aerodynamic forcing. They are randomly oriented in the horizontal plane, however. Electrostatic fields will disturb this situation by producing a torque on the filaments that will tend to align them along the field direction. By measuring the

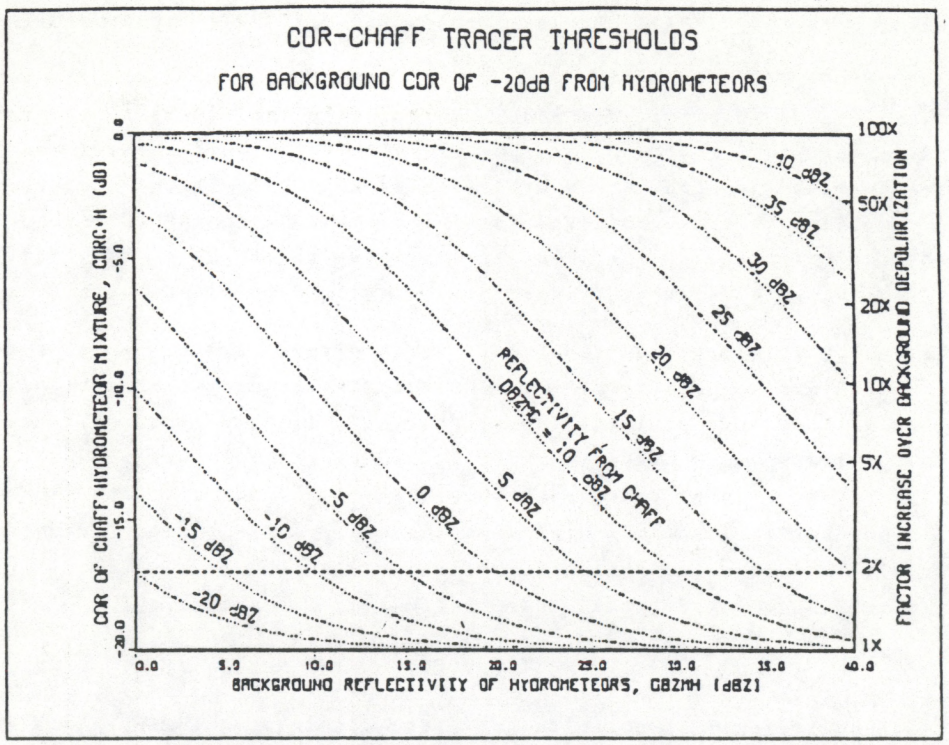

Figure 4. Graphical presentation of analytical solution to the equation for the circular depolarization ratio for a mixture of chaff and hydrometeors. Curved lines show the reflectivity which is required of chaff alone to produce CDR values of the mixture shown on the vertical axis for the background levels from hydrometeors of -20 dB CDR and reflectivities shown on the horizontal axis. The right-hand vertical axis displays the factor increase of the mixture CDR over the background CDR of the hydrometeors alone. Reflectivity of the chaff is directly related to the concentration of the chaff fibers.

amplitude and phase of the returned signal in both RH and LH receiver channels, we can obtain a measure of chaff orientation, the canting angle. The canting angle is the projection in the plane normal to the radar beam of the tilt angle of the particle's major axis from vertical. Since the component of the tilt within the vertical plane through the radar beam is not measured, a second radar some distance away would be needed to determine this component to unambiguously measure the true electric field direction. The canting angle, α, is related to the (complex) cross-covariance, W, between the RH and LH received signals by the relationship

$$W = \rho \exp(-2 j \alpha), \qquad (6)$$

where ρ is taken as the degree of common alignment of the chaff filament (McCormick and Hendry, 1979)[18]. The exact meaning of rho has been the subject of

[18]McCormick, C.G., and A. Hendry, 1979: Radar measurements of precipitation-related depolarization in thunderstorms. IEEE Trans. Geosci. Electron., 17, 142-150.

considerable discussion in the literature (Jameson, 1983[13]; Hendry and Antar, 1984[14]; Moninger et al., 1984[15]; McCormick and Hendry, 1979)[16]; however, there is general agreement about the meaning of alpha.

This technique is somewhat more problematical than the CDR technique for simply finding the chaff in the cloud; aerodynamic forces on the chaff need to be known better so that they can be compared with expected electrical torques. An additional complication arises because the introduction of chaff into an electrified cloud might alter the electrical properties of the cloud. This possible effect would need to be studied before such measurements were attempted.

A variation of this proposed technique, using natural hydrometeors, has been used by McCormick and Hendry (1979)[16] to infer the existence of electric fields and their subsequent breakdown by lightning discharge. This gives us confidence that the technique is feasible. Chaff filaments should be considerably more sensitive to electric fields than natural hydrometeors are; the filaments are long, thin, and electrically conductive, and thus will experience a greater torque. Providing strongly depolarized signals, the chaff will also make the results less dependent on the polarization quality of the radar system and, in particular, the antenna.

5. SUMMARY AND CONCLUSION

Chaff and dual (circular) polarization radar can be used to investigate a number of important atmospheric problems that involve the transport of air across cloud boundaries and the movement of air within clouds. The actual chaff concentration within the cloud can, under certain conditions, be determined from the reflectivity measured with the power received in the cross-polarized channel. Preliminary results indicate that the technique is feasible, at least in moderately reflecting clouds. Work is under way to demonstrate the method in clouds with higher reflectivities. Chaff can also be used to determine the electric field direction from the complex cross-covariance of the main- and cross-polarized signals.

Applications of these techniques include the venting of material from the planetary boundary layer by convective clouds, the direct observation of cloud-top entrainment and lateral entrainment of air into clouds, evaluation of the delivery of cloud seeding material into the desired region of clouds, and the transport of tropospheric air into the stratosphere by penetrating convective turrets.

---

[13]Jameson, A.R.,1983: Microphysical interpretation of multiparameter radar measurements in rain. Part I: Interpretation of polarization measure-ments and estimation of raindrop shapes. J. Atmos. Sci., 40, 1792-1802.

[14]Hendry, A., and Y.M.M. Antar, 1984: The variation of measured cross-polarized echo intensity in rain with direction of polarization, and its implication for canting angle distribution. Preprints, 22nd Conf. on Radar Meteorology, AMS, Boston, 382-386.

[15]Moninger, W.R., R.A. Kropfli, and F. Pasqualucci, 1984: Scattering properties of hydrometeors as measured by dual-polarization radar during CCOPE. Radio Sci., 19, 149-156.

Reprinted from JOURNAL OF ATMOSPHERIC AND OCEANIC TECHNOLOGY, Vol. 3, No. 2, June 1986
American Meteorological Society

Single Doppler Radar Measurements of Turbulence Profiles in the Convective Boundary Layer

R. A. KROPFLI

NOAA/ERL/Wave Propagation Laboratory, Boulder, CO 80303

(Manuscript received 22 February, in final form 12 November 1985)

ABSTRACT

The velocity-azimuth-display technique provides a measurement of the mean wind components above a conically scanning Doppler radar. Wind components are often computed from a least-squares fit of a sinusoid to the Doppler velocity-versus-azimuth data but it is not widely known that information about turbulence can also be obtained from such data. This paper demonstrates that the fluctuations of the measurements about the best-fit sinusoid are related to Reynolds stress components. These fluctuations, when computed about the mean from an ensemble of scans, provide estimates of stress that contain contributions from scales of motion from ~50 m to ~5 km. The method was tested with observations taken by the NOAA/WPL 3.2 and 0.86 cm wavelength radars in the dry, convective boundary layer in which small, naturally occurring particulates were used as tracers of the air motion. Results indicate that continuous profiles of wind and stress components can be produced from heights of about 200 m to the capping inversion (~2000 m) during periods of strong surface heat flux that occur in Colorado during the summer.

1. Introduction

A method described by Wilson (1970) relates second-order turbulence quantities to the fluctuations evident in a velocity-azimuth-display (VAD) analysis. This method is based on an earlier version by Lhermitte (1968), which utilized fixed-beam radar data to determine the variance of the longitudinal velocity and the covariance of the vertical and longitudinal velocities. We have implemented an extended version of Wilson's technique to include scales of motion much larger than those he described and have tested it with the NOAA/WPL 3.22 cm (X-band) and 0.86 cm (K-band) wavelength radars in the convective boundary layer (CBL) as well as in nonprecipitating clouds.

The CBL observations were made possible by the existence of particulate scatterers that serve as tracers of the air motion. These scatterers are present during the periods of strong upward heat flux at the surface that occur during the summer in Colorado. Although the exact nature of the scatterers is uncertain, we have reason to believe that the echoes result from small particles such as seeds, insects, and other millimeter-sized particles carried up from the surface by buoyant plumes and mixed by CBL turbulence.

Our experience has shown that from May through September the CBL in Colorado is usually filled with these naturally occurring echoes having equivalent X-band reflectivity factors ranging from −15 to +5 dBZ. There is no evidence that these scatterers have a mean self-induced motion since comparisons of horizontal velocities with measurements by anemometers on the Boulder Atmospheric Observatory (BAO) tower 3.5 km away show agreement to within about 0.2 m s^{-1}. In addition, the characteristic reflectivity pattern evident in radar displays when migrating insects are present (Schaefer, 1976) has not been observed. We conclude that the scatterers responsible for these echoes are passively carried aloft by the buoyant plumes and are assumed to be good tracers of the air motion in the discussions that follow.

The possibility that scatter from refractivity variations is responsible for these echoes has been ruled out because the observed X-band reflectivity factor is on the order of 40 dB too large. The S-band measurements of Chadwick et al. (1976) indicated that a mean equivalent X-band reflectivity factor of about −50 dBZ at the 800 m level is expected in northeast Colorado. The X-band echoes utilized here are much too strong to be caused by refractive index variations and are more in line with the X-band targets identified by Hardy and Katz (1969) as being insects and having a reflectivity factor of ~0 dBZ. In addition we have never observed a maximum in the reflectivity profile near the capping inversion; the existence of such a peak would be a good indication of refractivity scatter.

The vertical resolution of these measurements is a function of radar parameters such as the radar pulse

volume dimensions, range, elevation angle and range gate spacing. Typical parameters used in these studies were the following:

pulse length	37 or 75 m
beam width	0.5° or 0.8°
elevation angle	45° to 80°
range	<3 km
gate spacing	37 or 75 m.

Thus, independent measurements in the vertical can be achieved at about 40 to 70 m intervals, depending on the exact choice of radar parameters.

Horizontal scales of motion included in the estimates of Reynolds stress range from the small pulse-volume scale (~50 m) fluctuations to the larger-scale fluctuations observed in the wind components when a long sequence of scans is performed. If a 30 min averaging period is chosen, a 9 km sample of the CBL passes over the radar when the mean wind is 5 m s^{-1}. This should allow scales up to about 5 km or 10 km to be included in the stress measurements. Under typical conditions for which the CBL is 1 km deep, this sample would include the passage of several plumes.

The measurements described here include continuous profiles of the wind and Reynolds stress components throughout the depth of the CBL for durations of several hours. Such measurements are unattainable by other means. The spatial and temporal resolution and the precision of these first measurements appear to be suitable for applications that include studies of turbulence and diffusion as well as attempts to improve parameterizations of subgrid scale processes used in cloud and CBL models. Although the measurements described here were made with radar, the methods are transferable to any active remote sensing device that measures Doppler velocity, e.g., lidar and sodar.

2. Methodology

The VAD method for wind measurement at a fixed height (z) and time (t) utilizes the equation for the measured radial velocity V_R as a function of wind components (u, v, w) and the radar beam direction specified by azimuth (β) and elevation (θ):

$$V_R(\beta, \theta, t) = u(\beta, \theta, t) \sin\beta \cos\theta + v(\beta, \theta, t) \cos\beta \cos\theta + w(\beta, \theta, t) \sin\theta; \quad (1)$$

V_R is defined as positive for motions away from the radar. The z coordinate is not explicitly shown since we consider only measurements at a fixed height. Temporal variations are considered below. Browning and Wexler (1968) assumed a locally horizontally linear wind field such that at any height,

$$u = u_0 + x\left\langle\frac{\partial u}{\partial x}\right\rangle + y\left\langle\frac{\partial u}{\partial y}\right\rangle, \quad (2a)$$

$$v = v_0 + x\left\langle\frac{\partial v}{\partial x}\right\rangle + y\left\langle\frac{\partial v}{\partial y}\right\rangle, \quad (2b)$$

$$w = w_0, \quad (2c)$$

where u and v are the components along the x (east) and y (north) axis respectively, the vertical motion of the scatterers, w, is positive upward, the zero subscripts represent the components directly overhead ($x = 0$, $y = 0$), and angle brackets represent an average over a circle of radius R, where $R = z \cot\theta$ is the radius of the measurement circle swept out by a radar pulse volume during the conical scan.

Substitution of (2) into (1), as Browning and Wexler (1968) have done, yields the variation of V_R with azimuth for fixed height and elevation during conical (VAD) scanning. This expression is of the form

$$V_R(\beta, \theta, t) = A_{0t} + A_{1t} \sin\beta + A_{2t} \cos\beta + A_{3t} \sin 2\beta + A_{4t} \cos 2\beta \quad (3)$$

where the coefficients are evaluated at time t and are given by

$$A_{0t} = \frac{R}{2}\cos\theta\left(\left\langle\frac{\partial u}{\partial x}\right\rangle + \left\langle\frac{\partial v}{\partial y}\right\rangle\right) + w_0 \sin\theta,$$

$$A_{1t} = u_0 \cos\theta,$$

$$A_{2t} = v_0 \cos\theta,$$

$$A_{3t} = \frac{R}{2}\cos\theta\left(\left\langle\frac{\partial u}{\partial y}\right\rangle + \left\langle\frac{\partial v}{\partial x}\right\rangle\right),$$

$$A_{4t} = -\frac{R}{2}\cos\theta\left(\left\langle\frac{\partial u}{\partial x}\right\rangle - \left\langle\frac{\partial v}{\partial y}\right\rangle\right).$$

Measurements of $V_R(\beta)$ usually show this periodicity, and thus a harmonic analysis of $V_R(\beta)$ provides the following kinematic information over scales $> 2R$:

(i) a weighted sum of divergence, $\langle\partial u/\partial x\rangle + \langle\partial v/\partial y\rangle$, and vertical motion, w_0, from the zero-order harmonic.

(ii) the horizontal wind components u_0 and v_0 from the first-order harmonics.

(iii) stretching deformation, $\langle\partial u/\partial x\rangle - \langle\partial v/\partial y\rangle$, and shearing deformation, $\langle\partial v/\partial x\rangle + \langle\partial u/\partial y\rangle$, from the second-order harmonics.

In practice, a noisy sinusoidal variation of V_R with azimuth is observed; it is the result of large-scale ($>2R$) wind components, divergence and deformation. The superimposed noiselike signal is the result of small-scale ($<2R$) turbulence and random errors in the estimate of V_R. In addition, it is observed that when scans are repeated, the scan-to-scan fluctuations in u_0 and v_0 are too large to be measurement uncertainty and are therefore attributed to turbulence at scales $> 2R$.

An example of small-scale turbulence is given in Fig.

1. The data were taken in the CBL on 11 September 1983, with the NOAA/WPL X-band radar, and they represent samples from one range gate during a scan at an elevation of 60°. The least-squares fit of (3) to the data, also shown in the figure, provides an excellent measure of the wind components, u_0 and v_0. In addition the coefficient A_0 can provide a measure of w_0 when the elevation angle is high ($\cos^2\theta \ll 1$) and a measure of divergence when scanning at low elevation ($\sin\theta \ll 1$). Sixty degrees is an intermediate case, and a separation of w_0 and divergence cannot be made unless other elevations or assumptions are used.

There is usually a significant amount of scatter about the best-fit curve, and Fig. 1 is no exception. This scatter is not measurement uncertainty but is actually the turbulent signal important in many CBL studies. To verify this, the measurement uncertainty in V_R is estimated using the expression given by Dennenberg (1971):

$$\sigma^2 = \frac{\sigma_d \lambda}{8\sqrt{\pi} T}, \tag{4}$$

where σ^2 is the error variance of the estimate of V_R, σ_d is the width of the Doppler spectrum, and T is the dwell time or time to acquire a velocity sample. [This equation is valid when the signal-to-noise ratio is large (>10) as in the close-range observations described here.] Since a typical value for σ_d in the CBL is about 0.9 m s^{-1}, the 0.25 s dwell used in the X-band radar measurements of Fig. 1 yielded an uncertainty in V_R of 0.09 m s^{-1}. This error estimate is a small fraction of the fluctuations apparent in the figure and we conclude that the observed scatter represents turbulence at scales larger than the radar pulse volume and smaller than $2R$.

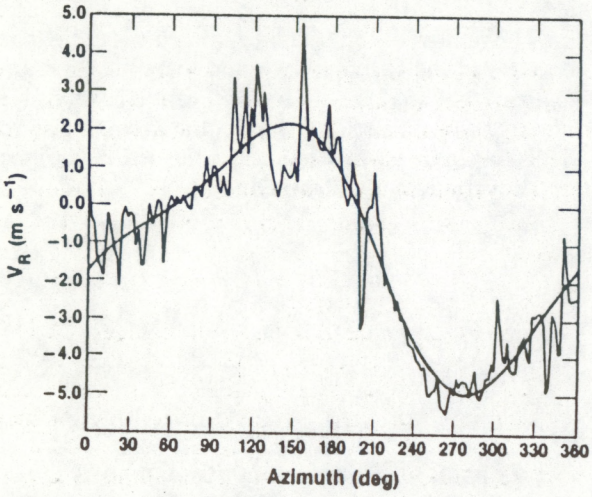

FIG. 1. Radial velocity vs azimuth, showing the effects of the (single-scan) mean wind and small-scale (<2R) turbulence. Data were from the 60° X-band scans at 1150 MST on 11 September 1983 at a height of 42° m. The least-squares-fit to (3) is indicated.

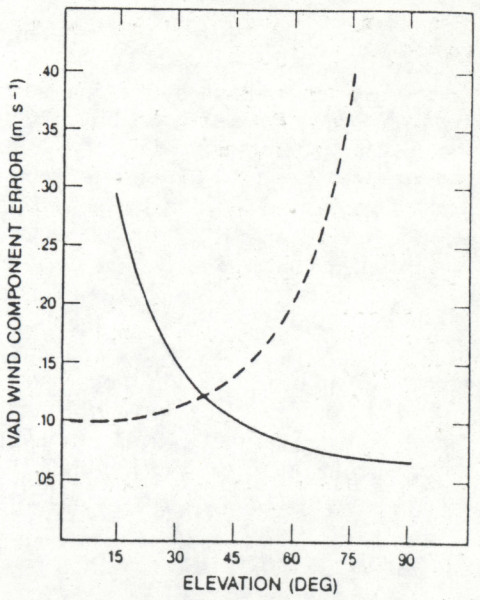

FIG. 2. Error estimates of the wind components derived from least-squares-fit analysis of VAD data. Two hundred rays of data and a 1 m s^{-1} standard deviation of V_R about the best-fit curve were assumed. The dashed curve represents the error in either horizontal wind component, and the solid curve is the error in $w(z)$ when $\mathrm{div}(z) \approx 0$.

The observed scan-to-scan fluctuations in wind components are now shown to be too large to be caused by measurement uncertainty and are therefore the result of turbulence at scales > $2R$. Expected errors for will be dropped from here on) determined from the "measurement matrix" of the least-squares-fit analysis (Mathews and Walker, 1965) are found to be the following:

$$\sigma_u = \sigma_v = \left(\frac{2\,\mathrm{VAR}(V_R)}{n}\right)^{1/2} \sec\theta \tag{5a}$$

$$\sigma_w = \left(\frac{\mathrm{VAR}(V_R)}{n}\right)^{1/2} \csc\theta. \tag{5b}$$

In these expressions n is the number of measurements of V_R used in the least-squares analysis and $\mathrm{VAR}(V_R)$ is the scatter of data about the single-scan least-squares fit. Note that (5b) applies when the divergence term in A_0 is small ($\mathrm{div} \sim 0$ or $\theta \gtrsim 70°$). Single-scan velocity errors are plotted as a function of θ in Fig. 2 for $\mathrm{VAR}(V_R) = 1$ m^2 s^{-2} and $n = 200$. These are typical values in the examples that follow. These errors are caused by the total scatter about the best-fit curve resulting from small-scale turbulence as well as the uncertainty in the estimate of V_R given by (4). Note that these errors in the wind components are ~0.1 m s^{-1} over a wide range of elevation angles and are an order of magnitude smaller than typical turbulent fluctuations in the CBL.

If one performs a series of scans to establish a time-averaged wind component, a record similar to that shown in Fig. 3 is produced. The fluctuations seen in such a record are caused mostly by large-scale turbulence and to a lesser extent by the single-scan uncertainty given by (5). These fluctuations are interpreted as the passage of "frozen turbulence" over the radar in the same way Taylor's hypothesis is usually applied to in situ data. Wilson (1970) described a technique in which the small-scale ($<2R$) turbulent fluctuations shown in Fig. 1 could be used to estimate Reynolds stress components from a single scan. Application of this technique to fluctuations about the mean derived from an ensemble of scans, as in Fig. 3, allows scales larger than $2R$ to be included in the estimates.

Instead of considering the fluctuations of V_R about the mean sinusoid estimated from a single scan, we consider here the fluctuations of V_R about a long-term mean over a period T_0. This is expressed as

$$\text{var}[V_R(\beta, \theta)] = \overline{[V'_R(\beta, \theta, t)]^2}$$

$$= \overline{[V_R(\beta, \theta, t) - \overline{V_R(\beta, \theta, t)}]^2} \quad (6)$$

where

$$(\bar{\ }) \equiv \frac{1}{T_0}\int_0^{T_0} (\ )dt.$$

This temporal average is approximated by a summation over N scans:

$$\overline{V_R(\beta, \theta, t)} \approx \frac{1}{N}\sum_{i=1}^{N} V_R(\beta, \theta, i)$$

$$\approx \frac{1}{N}\sum_{i=1}^{N} (A_{0i} + A_{1i}\sin\beta + A_{2i}\cos\beta$$

$$+ A_{3i}\sin 2\beta + A_{4i}\cos 2\beta) \quad (7)$$

where $V_R(\beta, \theta, i)$ is derived from the Fourier coefficients of the ith scan as shown. The variance about this ensemble mean is computed in the same way that Wilson (1970) used the single-scan mean. The resulting variance equation is as follows:

$$\text{var}(V_R) = \text{var}(u)\cos^2\theta\sin^2\beta + \text{var}(v)\cos^2\theta\cos^2\beta$$

$$+ \text{var}(w)\sin^2\theta + \text{cov}(uv)\cos^2\theta\sin 2\beta$$

$$+ \text{cov}(uw)\sin 2\theta\sin\beta + \text{cov}(vw)\sin 2\theta\cos\beta. \quad (8)$$

We have used the notation $\overline{u'v'} \equiv \text{cov}(uv)$, etc. This equation is the same as that given by Wilson (1970); however, when $\text{var}(V_R)$ is computed about the ensemble mean the variances and covariances in (8) include contributions from larger scale ($>2R$) motions as well as from smaller scales ($<2R$).

It is apparent from (8) that the desired variances and covariances can be computed by a Fourier analysis of the $\text{var}[V_R(\beta)]$. However, Wilson (1970) described a mathematically equivalent way of performing this calculation that is computationally simpler. The $\text{var}(V_R)$ is weighted by odd and even square wave functions with the same result as that obtained from a Fourier analysis. In applying this method, four integrals, one for each quadrant, are computed from the deviations of $V_R(\beta, \theta, i)$ about the sinusoid derived from the coefficients

$$\bar{A}_0 = \frac{1}{N}\sum_{i=1}^{N} A_{0i}, \quad \bar{A}_1 = \frac{1}{N}\sum_{i=1}^{N} A_{1i},$$

etc., as described above. These integrals are

$$I_1 = \int_0^{\pi/2} \text{var}(V_R)d\beta; \quad I_2 = \int_{\pi/2}^{\pi} \text{var}(V_R)d\beta;$$

$$I_3 = \int_{\pi}^{3\pi/2} \text{var}(V_R)d\beta; \quad I_4 = \int_{3\pi/2}^{2\pi} \text{var}(V_R)d\beta. \quad (9)$$

Assume now that the turbulence is horizontally homogeneous, i.e., that the variances and covariances of u, v and w are therefore independent of azimuth and may be removed from the integrals; this is expected to be valid in the CBL except when there are kinematic features that are fixed to the terrain. We have also implicitly assumed stationarity over the averaging period. Thus the following expressions for the desired variances and covariances are obtained:

$$\text{var}(u) + \text{var}(v) + 2\tan^2\theta\,\text{var}(w)$$

$$= (I_1 + I_2 + I_3 + I_4)(\pi\cos^2\theta)^{-1} \quad (10a)$$

$$\text{cov}(uw) = [(I_1 + I_2) - (I_3 + I_4)](4\sin 2\theta)^{-1} \quad (10b)$$

$$\text{cov}(vw) = [(I_4 + I_1) - (I_2 + I_3)](4\sin 2\theta)^{-1} \quad (10c)$$

$$\text{cov}(uv) = [(I_1 + I_3) - (I_2 + I_4)](4\cos^2\theta)^{-1}. \quad (10d)$$

As a point of clarification, this is not an "eddy correlation" technique in which u' and w' are separately derived to obtain their correlation. These turbulent velocity correlations are derived from their effect on

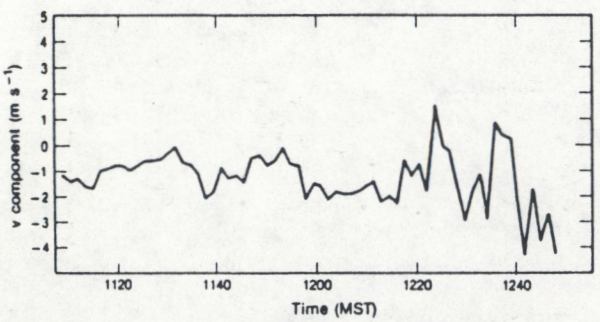

FIG. 3. Westerly (v) component vs time showing the effect of larger scale ($>2R$) turbulence. Data were from the 60° X-band scans on 11 September 1983, at a height of 420 m with samples every 90 s.

var(V_R) as in (8). It is possible to extend this procedure to triple products by a similar analysis of the quantity $\overline{[V_R - \bar{V}_R]^3}$, though no attempt is made to do so here.

Scan strategies designed to measure wind components and second-order turbulence quantities can be made on the basis of the covariance equations (10) and the expected errors in wind components (5). For example from (10b) we see that the elevation dependent factor $(4 \sin 2\theta)^{-1}$ is a maximum at $\theta = 45°$ which produces a minimum error in cov(uw) and cov(vw). As expected, (5a) and (5b) show error minima at $\theta = 0°$ and $\theta = 90°$ for horizontal and vertical components respectively. No single elevation is optimum for all relevant quantities.

3. Demonstrations of validity

As a demonstration of the precision of these measurements, a set of synchronized VAD scans was obtained with the NOAA/WPL K-band and X-band radars when they were colocated and scanning at high elevation angles in a nonprecipitating cloud at close range. Cloud data are presented here because CBL data were not taken while the radars were colocated. Wind and second-order turbulence quantities were independently derived from single scan data from each radar. Scatter plots of X-band estimates are plotted against K-band estimates in Figs. 4a and 4b for u and cov(uw) respectively. Each point in the figures was derived for each radar from the same range gate (or height) during identical and simultaneous scans while the radars were colocated.

Table 1 summarizes the rms differences between independent measurements with each radar, derived from the data shown in Figs. 4a and 4b. These measured differences are consistent with the computed velocity errors illustrated in Fig. 2, and they show the expected elevation dependency for the covariances. These results indicate that the precision of the technique is excellent and comparable with that achieved using "tower-quality" instrumentation.

Measurements obtained described here indicate that stress is roughly proportional to the negative of the shear in the CBL only when the shear exceeds $\sim 5 \times 10^{-3}$ s^{-1}. Figure 5 indicates this during a time when shear exceeded this value through a depth of 1 km for more than 100 minutes. The profiles of v and cov(vw)

TABLE 1. Rms differences in m s^{-1} derived from simultaneous VAD scans with two colocated radars.

Elevation (deg)	ϵ_u	ϵ_w	ϵ_{uw}	ϵ_{vw}
45	0.07	0.04	0.04	0.08
60	0.08	0.03	0.07	0.22
75	0.20	0.03	0.11	0.41

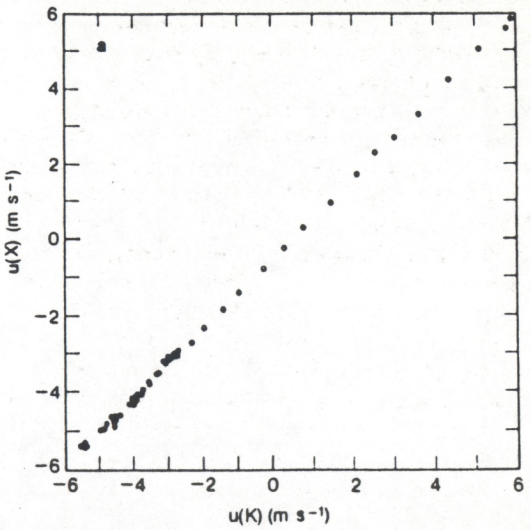

FIG. 4. Scatter plot of (a) u component and (b) cov(uw) at corresponding range gates derived from colocated X-band and K-band radars scanning simultaneously at 45° elevation at 1441 on 7 February 1984.

in this figure show correspondence between levels where $\partial v/\partial z < 0$, and cov($vw$) > 0, where $\partial v/\partial z \sim 0$ and cov(vw) $\sim$ 0, and where $\partial v/\partial z > 0$ and cov(vw) < 0. Under these highly sheared conditions therefore, the eddy diffusivity concept seems appropriate as shown in Table 2. These eddy diffusivities were computed from shear and stress profiles between 210 and 980 m for successive 20 min averages on 27 September 1982, the same data included in Fig. 5. Missing values in the table result from the smaller magnitudes of stress and shear that make their ratio indeterminate. Most other values appear reasonable in comparison with the

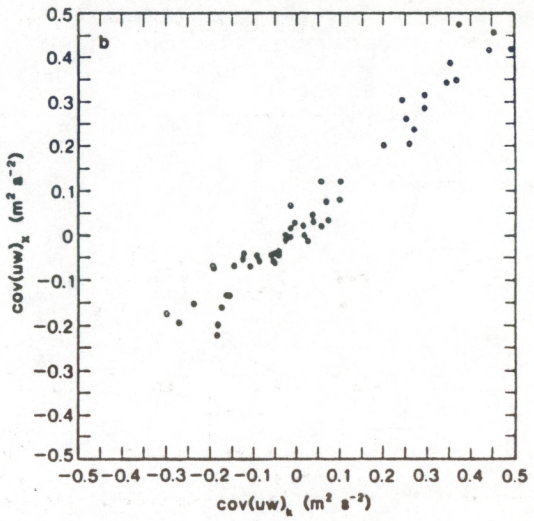

FIG. 4b. As in Fig. 4a but for cov(uw).

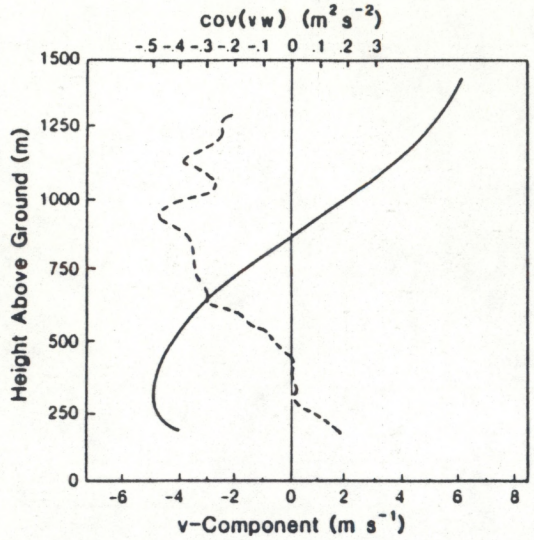

FIG. 5. Profiles of v (solid) and cov(vw) (dashed) for a 100 min period beginning at 1203 MST on 27 September 1982, obtained with X-band radar scanning at 45° elevation.

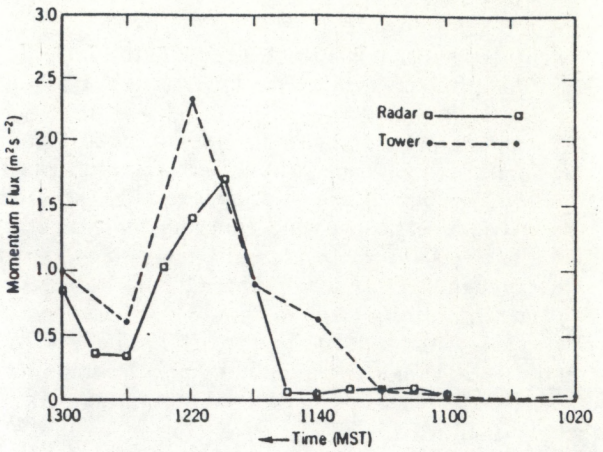

FIG. 6. Tower and radar estimates of vertical flux of horizontal momentum vs time on 11 September 1983. These are 20 min averages near the 300 m level computed for the 60° elevation scans. Radar plot is advanced by 10 min.

value of ~70 m² s⁻¹ suggested by Draxler (1979) for the CBL with moderate insolation and a wind speed of 4 to 6 m s⁻¹. The large variability in K_u reflects the weaker shear in the easterly direction.

The best opportunity to compare turbulence measurements from two separated instruments in the CBL occurs when the mean wind is along the line between them (Haugen et al., 1975). Such an opportunity occurred on 11 September 1983 when the NOAA/WPL X-band radar was located 3.5 km east of the BAO and the mean wind direction was only about 15° off the line of sight between them. Figure 6 shows radar and tower estimates of the vertical flux of horizontal momentum as a function of time. The radar values are near the 300 m level, the height at which the tower samples are made, and have been advanced by 10 min as seems appropriate from the mean wind of 6 m s⁻¹ and the 3.5 km distance between sensors. The plotted data represent 20 min averages and the radar data are computed and plotted every 10 min. The similarity suggests that both measurement techniques are responding to the same turbulent signal. These data are shown here as a demonstration that the radar technique produces credible results; they will be discussed in more detail in section 4.

TABLE 2. Eddy diffusivity estimates.

Time	K_u (m² s⁻¹)	K_v (m² s⁻¹)
1151	—	35
1159	—	50
1211	—	55
1232	81	52
1240	37	54
1304	235	26
1319	117	−16
1339	68	36
Average	107	36

4. A case study

(a) Observations of winds and stress

During the continuous conical scans on 11 September 1983, a weak trough passed through the area and was well documented with profiles from the VAD method. This trough was associated with a weak, low pressure center moving through South Dakota. For 2½ hours the radar performed conical scans alternating between 60° and 80° elevation, each scan taking 45 s. Figure 7 illustrates the time–height cross section of the observed wind profiles from the 60° scans plotted as vectors. As noted earlier, estimates of w made at $\theta = 60°$ can be degraded by the contribution from divergence. Comparisons of these 60° data with estimates of w taken at 80°, however, are in good agreement here. (Figure 10, discussed later, is an example of one such comparison.) The vectors displayed at 1.5 min intervals have components given by u and w after 6 m s⁻¹ was subtracted from the u component to show the wind in a coordinate system moving with the mean wind. The usable echo extends to about 2 km for most of the period.

The presence of radar echoes to a height of 2 km during the period of stability before 1135 MST is not completely understood but may have been caused by chaff that had been distributed at the surface on pre-

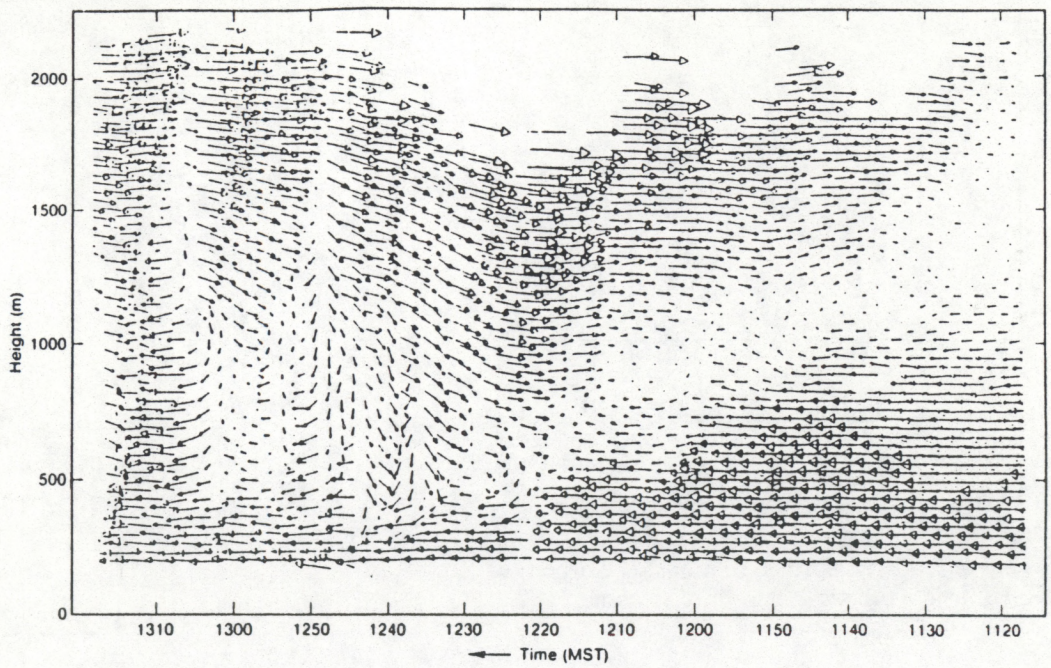

FIG. 7. Time–height cross section of the u, w wind vector field constructed from 60° elevation conical scans every 90 s. The mean wind speed of 6 m s^{-1} has been subtracted from the u component. A vector of length equivalent to 5 min on the time scale represents 6 m s^{-1}.

vious days for a different experiment. The spatial distribution of these echoes was similar to individually resolved point targets rather than from the more continuously distributed structure expected from refractive index variations. In addition, the earlier discussion about the relative signal intensities applies here as well and leads to the conclusion that refractivity scatter is not contributing to these data. This chaff could have been recirculated by the mesoscale wind pattern to cause the 2 km-deep echo prior to 1200 MST. Figure 7 shows that this stable period was characterized by relatively weak vertical mixing, i.e., weak vertical motions, and also by high shear ($\sim 5 \times 10^{-3}$ s^{-1}).

Data from the BAO acoustic sounder (Fig. 8) indicated that the CBL grew slowly to a height of about 300 m by 1030 and then decreased to a height of 190 m by 1100. The dark wavelike trace represents the capping inversion at the top of the CBL. Shortly after 1100 the capping inversion disappeared from the acoustic sounder record, consistent with potential temperature data from the BAO (Fig. 9) that show the capping inversion weakening and rising after 1100. In Fig. 9 contours of potential temperature are plotted as a time–height cross section. The dashed line at the upper right is the height of the inversion from 10 min averages of tower data. The dashed, nearly vertical line at about 1220 separates easterly flow before 1220 from the westerly flow that occurred later. These data suggest

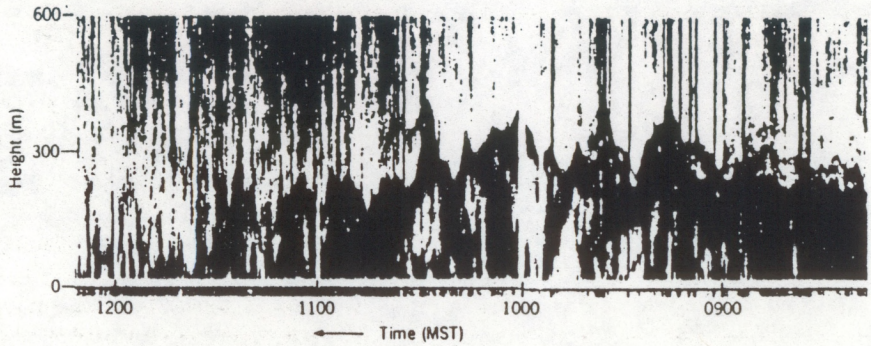

FIG. 8. BAO acoustic sounder record for 11 September 1983.

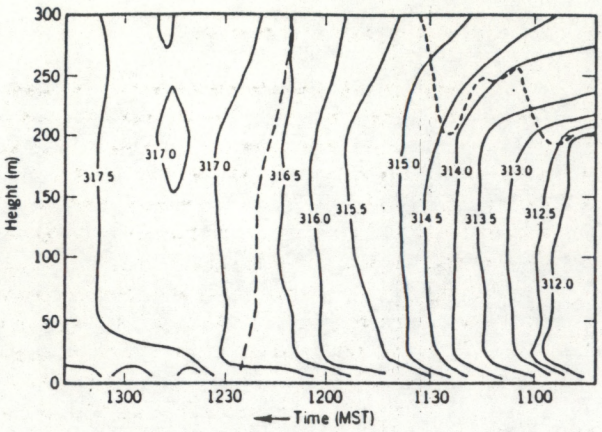

FIG. 9. Time-height cross section for potential temperature at BAO on 11 September 1983. Dashed line at the upper right is the inversion base and dashed line at ~1220 separates easterly flow (on the right) from westerly flow (on the left).

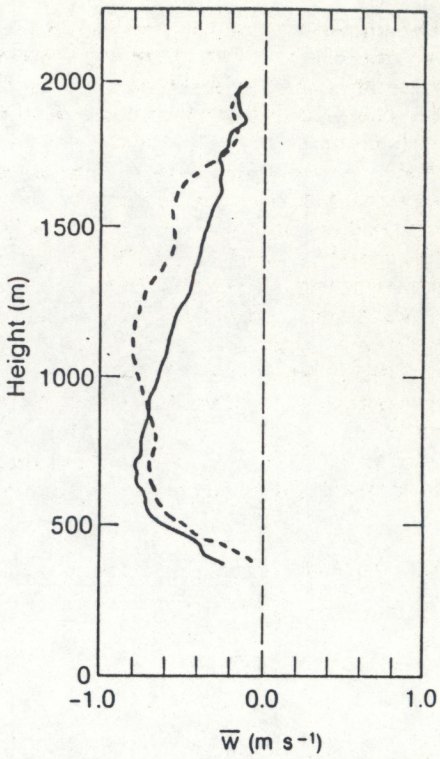

FIG. 10. Profiles of w from the 80° (solid) and 60° (dashed) elevation scans for the 70-min period beginning at 1221 MST.

that buoyancy driven vertical motions would be suppressed at heights above 200 m prior to about 1130 at the BAO.

The 80° elevation radar data indicate that a downdraft in excess of 2.5 m s^{-1} occurred at the 600 m level from 1232 to 1244 MST. A steady downdraft of 0.8 m s^{-1} was also observed for a 35 min period at the 300 m level of the BAO tower shortly after the wind shift shown by the dashed line in Fig. 9.

Figure 10 shows w profiles derived from the 60° and 80° scans averaged from 1221 to 1331 MST. Both profiles show a 0.8 m s^{-1} persistent downdraft near the 600 m level. (The average of w during the previous hour was near zero.) The agreement of these two independent radar profiles and the BAO data gives reassurance that the measurements are correct and that unexpected features such as strong and persistent mesoscale downdrafts can exist in the CBL.

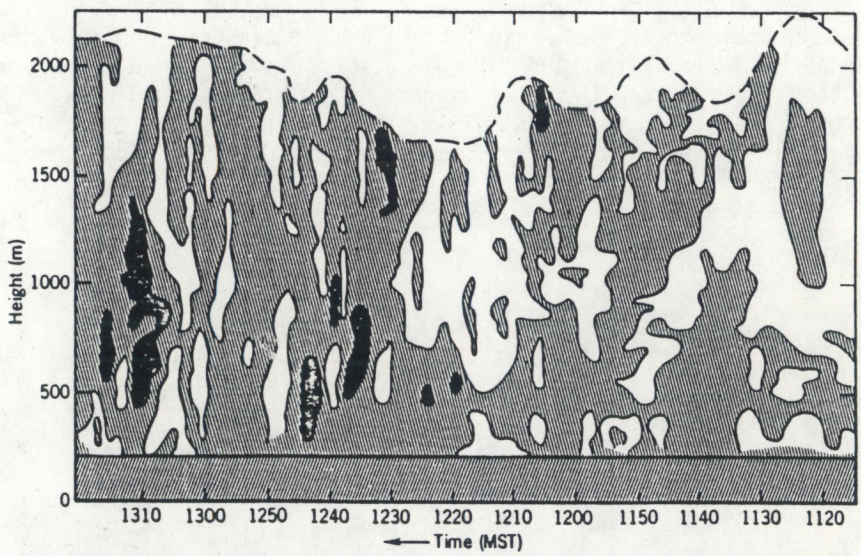

FIG. 11. Time-height cross section for cov(uw) indicating the positive (clear) and negative (hatched) values. Shaded areas represent values of cov(uw) < −3 m^2 s^{-2}. Solid horizontal line at 200 m indicates lower boundary of data.

The time–height plot of cov(uw) in Fig. 11 clearly shows the effect of the more vigorous momentum transfer after the low-level stable layer had eroded away. This record shows that the vertical transport of easterly momentum was effectively suppressed during the stable first-half of the record when values of cov(uw) never exceeded ± 1 m^2 s^{-2}. Nevertheless, the record shows good continuity in time and in height.

The unstable period after 1220 was characterized by much larger variations in |cov(uw)| and magnitudes of downward transfer of momentum often exceeded 3 m^2 s^{-2} as shown by the shaded areas. It is also seen that the patches of large covariance are vertically elongated in contrast to the earlier stable period. Twenty minute averages of surface temperature flux ranged from 0.15°C to 0.22°C m s^{-1} during these measurements and are typical for convective conditions at the BAO.

(b) Insights into eddy diffusivity

The data provide an interesting test of the eddy diffusivity concept since a variety of stability and shear conditions are present. The u component was highly sheared, having an average shear of about 5×10^{-3} s^{-1} over a 2000 m depth, the v component had very little mean shear over this depth, and as we have seen, the data encompassed a stable and an unstable regime. Profiles of the wind components and their corresponding covariances are shown in Figs. 12. Profiles in Figs. 12a and 12b for the weakly sheared v component, are computed for 70 min periods starting at 1109 (stable) and 1221 (unstable). Figures 12c and 12d show the highly sheared u component for the same periods.

It is apparent that an eddy diffusivity formulation would be appropriate only for Fig. 12d, the sheared,

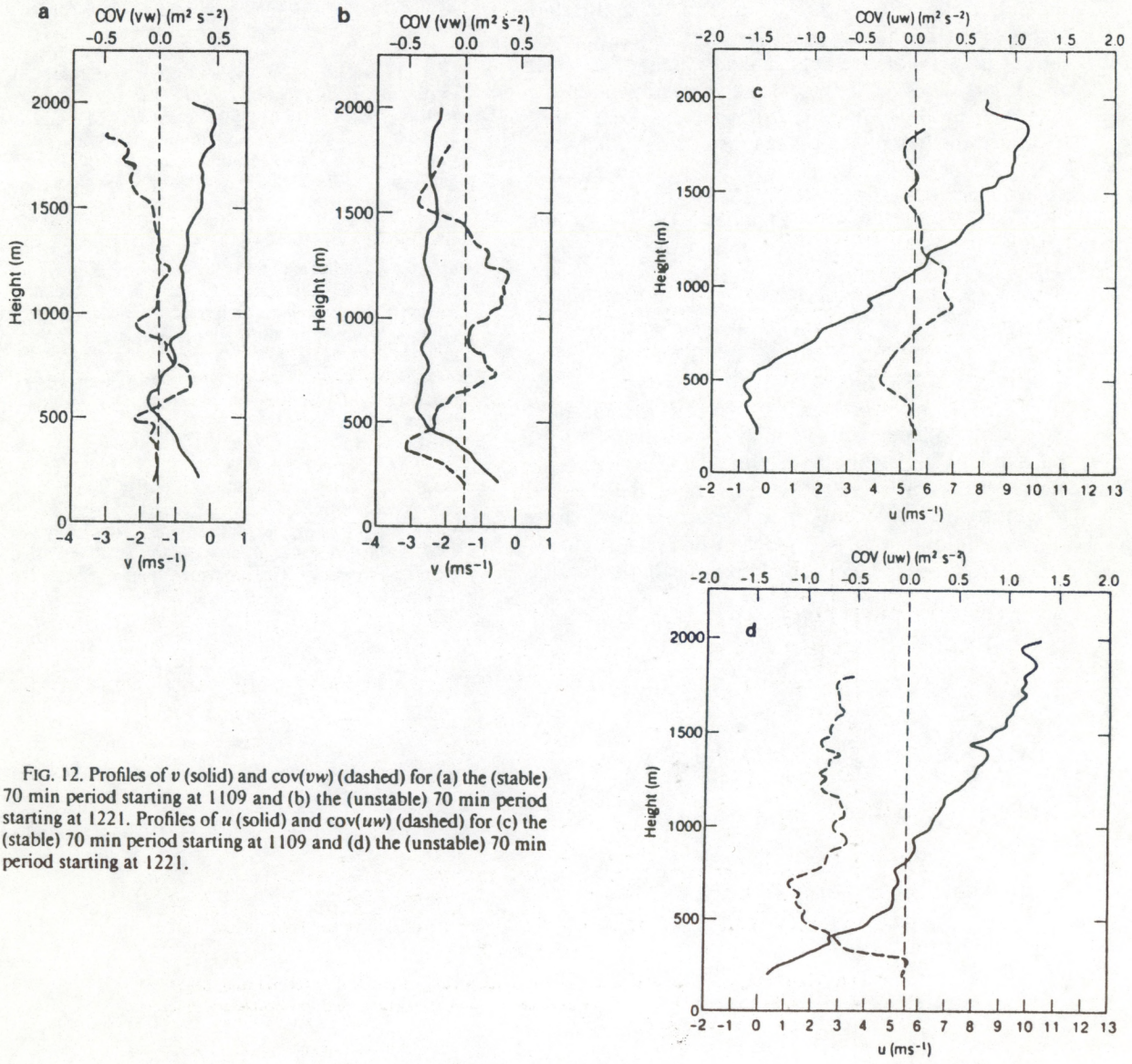

FIG. 12. Profiles of v (solid) and cov(vw) (dashed) for (a) the (stable) 70 min period starting at 1109 and (b) the (unstable) 70 min period starting at 1221. Profiles of u (solid) and cov(uw) (dashed) for (c) the (stable) 70 min period starting at 1109 and (d) the (unstable) 70 min period starting at 1221.

unstable case. The other three situations are either too stable for significant vertical mixing (Figs. 12a and 12c) or have too little shear (Fig. 12b) for eddy diffusivity to be useful. It appears then, that in addition to the high shear mentioned earlier with regard to other datasets, the absence of strong stability is an additional requirement for shear and stress to be approximately proportional.

5. Summary

The method described by Wilson (1970) for turbulence measurements with radar has been extended to include contributions from larger scales. Excellent opportunities to use this technique occur at short range and high elevation when horizontally homogeneous echoes occur in the visually clear CBL and stratus clouds.

We have found that such echoes are frequently observable in the CBL with K-band and X-band radars from May through September in Colorado, even though these radars are not usually thought of as "clear air" radars. These echoes are usually not present during the winter months when the atmosphere is more stable. It is most likely that the echoes result from small particles such as seeds, insects and other millimeter-sized particles carried up from the surface by buoyant plumes and turbulence in the CBL when the surface heat flux is large. These particulates are found to be excellent tracers of the air motions.

Analysis of several datasets suggests that this radar technique can provide velocity profiles with errors as small as 5 cm s^{-1} and profiles of turbulent velocity covariances with errors on the order of 0.04 $m^2 s^{-2}$ to heights of 2 km or greater. The vertical resolution is good with independent samples about every 50 m. Horizontal scales included in the second-order quantities range from about 50 m to greater than 5 km. Therefore, under the conditions described here, these radar techniques can be used to provide turbulence data that compare favorably with data that would be obtained from a 2 km high instrumented tower. The observations of wind and stress described here illustrate the good potential for this new radar technique to reveal the structure of the CBL.

Acknowledgments. The author would like to thank Douglas Lilly for asking the stimulating questions that renewed interest in the use of Doppler radar for turbulence measurements. The comments and suggestions of Jay Miller and Peter Hildebrand are also greatly appreciated. Willian Neff provided the acoustic sounder data and Thomas Lefevre provided the BAO potential temperature data. Improvements in the software package used here were implemented by James Geschke and David Woodward and much of the radar data processing was performed by Troy Gieser.

REFERENCES

Browning, K. A., and R. Wexler, 1968: The determination of kinematic properties of a wind field using a Doppler radar. *J. Appl. Meteor.*, **7**, 105–113.

Chadwick, R. B., K. P. Moran, R. G. Strauch, G. E. Morrison and W. C. Campbell, 1976: Microwave radar wind measurements in the clear air. *Radio Sci.*, **11**, 795–802.

Dennenberg, J. N., 1971: The estimation of spectral moments. Tech. Rep. No. 23, Laboratory for Atmospheric Probing, University of Chicago and Illinois Institute of Technology, 79 pp.

Draxler, R. R., 1979: Estimating vertical diffusion from routine meteorological tower measurements. *Atmos. Environ.*, **13**, 1559–1564.

Hardy, K. R., and I. Katz, 1969: Probing the clear atmosphere with high power, high resolution radars. *Proc. IEEE*, **27**, 468–480.

Haugen, D. A., J. C. Kaimal, J. C. Readings and R. Rayment, 1975: A comparison of balloon-borne and tower-mounted instrumentation for probing the atmospheric boundary layer. *J. Appl. Meteor.*, **14**, 540–545.

Lhermitte, R. M., 1968: Turbulent air motion as observed by Doppler radar. *Proc. 13th Conf. on Radar Meteorology*, Montreal, Amer. Meteor. Soc., 498–503.

Mathews, J., and R. L. Walker, 1965: *Mathematical Methods of Physics*. W. A. Benjamin, 475 pp.

Schaefer, G. W., 1976: Radar observations of insect flight. *Insect Flight*, R. C. Rainey, Ed., Halsted Press, Wiley, 157–197.

Wilson, D. A., 1970: Doppler radar studies of boundary layer wind profiles and turbulence in snow conditions. *Proc. 14th Conf. on Radar Meteorology*, Tuscon, Amer. Meteor. Soc., 191–196.